ATTACHMENT D
PASSIVE EQUIPMENT FAILURE ANALYSIS

INTENTIONALLY LEFT BLANK

CONTENTS

Page

INTENTIONALLY LEFT BLANK

FIGURES

Page

INTENTIONALLY LEFT BLANK

TABLES

Page

TABLES (Continued)

Page

ACRONYMS AND ABBREVIATIONS

Acronyms

CDF	cumulative distribution function
COV	coefficient of variation
CRCF	Canister Receipt and Closure Facility
CTM	canister transfer machine
DOE	U.S. Department of Energy
DPC	dual-purpose canister
EPS	equivalent (or effective) plastic strain
ETF	expended toughness fraction
FEA	finite element analysis
GROA	geologic repository operations area
HLW	high-level radioactive waste
INL	Idaho National Laboratory
LLNL	Lawrence Livermore National Laboratory
LOS	loss of shielding
LS-DYNA	Livermore Software–Dynamic Finite Element Program
MCO	multicanister overpack
NAC	Nuclear Assurance Corporation
OCB	outer corrosion barrier
PCSA	preclosure safety analysis
PDF	probability density function
SAR	Safety Analysis Report
SLS	steel-lead-steel
SNF	spent nuclear fuel
STC	shielded transfer cask
TAD	transportation, aging, and disposal
TEV	transport and emplacement vehicle
WHF	Wet Handling Facility
WPTT	waste package transfer trolley
YMP	Yucca Mountain Project

ACRONYMS AND ABBREVIATIONS (Continued)

Abbreviations

°C	degrees Celsius
cm	centimeter
°F	degrees Fahrenheit
ft	foot, feet
hr, hrs	hour, hours
J	joule
K	Kelvin
kg	kilogram
kV	kilovolt
kW	kilowatt
m	meter
min	minute, minutes
mrem	millirem
MPa	megapascal
mph	miles per hour
psig	pounds per square inch gauge
rem	roentgen equivalent man
sec	second, seconds
W/m K	watt per meter Kelvin
W/m^2K	watt per square meter Kelvin

ATTACHMENT D
PASSIVE EQUIPMENT FAILURE ANALYSIS

Many event sequences described in Section 6.1 include pivotal events that arise from loss of integrity of a passive component, namely one of the aging overpacks, casks, or canisters that contain a radioactive waste form. Such pivotal events involve (1) loss of containment of radioactive material that may result in airborne releases, or (2) loss of shielding effectiveness. Both types of pivotal events may be failure modes caused by either physical impact to the container or by thermal energy transferred to the container. This attachment presents the results of passive failure analyses that provide conditional probability of loss of containment or loss of shielding. Many scenarios were selected for analysis as representative or bounding for anticipated scenarios in the risk assessment. Results of some scenarios may not have been used in the final event sequence quantification.

D1 LOSS OF CONTAINMENT DUE TO DROPS AND IMPACTS

The category of passive equipment includes canisters and casks used during transport, aging, and disposal of spent nuclear fuel. The canisters and casks contain the spent fuel and provide containment of radioactive material. During transport and handling, the canisters and casks could be subjected to drops, impacts, or fires, which may result in loss of containment. The probabilities of loss of containment due to various physical or thermal challenges are evaluated primarily through structural and thermal analysis and drop test data.

Passive equipment (e.g., transportation casks, storage canisters, and waste packages) may fail from abnormal use such as defined by the event sequences. Studies were performed and passive equipment failure probabilities were determined using the methodologies summarized in Section 4.3.2.2. The probability of loss of containment (breach) was determined for several types of containers, including transportation casks (analyzed without impact limiters), shielded transfer casks, waste packages, transportation, aging, and disposal (TAD) canisters, dual-purpose canister (DPCs), U.S. Department of Energy (DOE) standardized canisters, multicanister overpacks (MCOs), high-level radioactive waste (HLW) canisters, and naval spent nuclear fuel (SNF) canisters. The mechanical breach of TAD canisters, DPCs and naval SNF canisters were analyzed as representative canisters as described in Section D1.1. The structural analysis of DOE standardized canisters and MCOs for breaches is described in Section D1.2 and then the probabilistic methodology of Section D1.1 was applied. Transportation casks, shielded transfer casks (STCs) and horizontal STCs were analyzed as representative transportation casks as describe in Section D1.1. The probabilistic estimation of breach from mechanical loads of all other waste containers is described in Sections D1.3 through D1.6. The analysis of loss or degradation of shielding of casks and overpacks against mechanical loads is described in Section D3. The probabilistic analysis of fire severity and the associated effects on casks, canisters, and overpacks with respect to both containment breach and shielding degradation or loss is described in Section D2. The analysis of mechanical failures and thermal failures included the specific configuration defined by the event sequences. For example, if the event sequence occurred during a process in which the canister is within a transportation casks or aging overpack, the analysis is performed in that configuration.

D1.1 LAWRENCE LIVERMORE NATIONAL LABORATORY ANALYSIS OF CANISTERS AND CASKS

Lawrence Livermore National Laboratory (LLNL) performed the finite element analysis (FEA) using Livermore Software–Dynamic Finite Element Program (LS-DYNA) to model drops and impacts for casks and canisters with selected properties for use as representative containers expected to be delivered to Yucca Mountain (Ref. D4.1.27). LS-DYNA, which has been used in nuclear facility and non-nuclear industrial applications, is appropriate to model nonlinear, transient responses of a passive component to a structural challenge such as a drop or an impact. Existing commercial casks and canisters that would likely be used on the Yucca Mountain Project (YMP) were identified and characterized. The cases analyzed are listed in Table D1.2-1.

Appropriate finite element models were developed for the representative cask, selected container types, configurations, and drop types. The level of detail for each model was selected to understand deformation and damage patterns, possible failure mode(s) in each structural element, and failure-related response. Special attention was required to properly model the bottom-weld and closure regions to ensure that coarser mesh of the simplified model would capture failure-related response with acceptable accuracy. A consistent failure criterion for each case was identified as part of the detailed analyses. The effective plastic strain in each element, in combination with material ductility data, was used to predict failure measures.

The maximum strain for each scenario was compared with the capacity distribution based on material properties to obtain containment failure probabilities using the methodology described in Section 4.3.2.2. For simplicity and consistency in interpreting results, the impact-surface conditions, including both the ground and the falling 10-ton load for the analyses, were considered infinitely stiff and unyielding, which is conservative.

The results of these cases are summarized in Tables D1.2-2 through D1.2-4. The bases for these results are summarized in the following paragraphs. If a probability for the event sequence is less than 1.0×10^{-8}, additional conservatism is incorporated in the preclosure safety analysis (PCSA) by using a failure probability of 1.0×10^{-5}, which are termed "LLNL, adjusted". This additional conservatism is added to account for a) future evolutions of cask and canister designs, and b) uncertainties, such as undetected material defects, undetected manufacturing deviations, and undetected damage associated with handling before the container reaches the repository, which are not included in the tensile elongation data.

LLNL developed a fragility curve for the base metal by fitting a mixture of two normal probability density functions (PDFs) to the engineering (tensile) strain data (Ref. D4.1.4). Both the data and their corresponding log-transforms were found to be non-normally distributed ($p < 10^{-4}$) by the Shapiro-Wilk test (Ref. D4.1.62). These data collected at 100°F were determined to be reasonably well modeled as a sample from a weighted mixture of two normal distributions, one with a mean of 46 % and a standard deviation of 2.24 % (weight = 7.84 %), and the other with a mean of 59.3 % and a standard deviation of 4.22 % (weight = 92.16 %), with the goodness of fit ($p = 0.939$) assessed by the Kolmogorov-Smirnov 1 sample test (Ref. D4.1.33).

The stainless steel used in the LLNL (Ref. D4.1.27) analysis is alloy 304L. The un-annealed alloys have relatively shorter elongations at failure than annealed 304L as shown in Figure D1.1-1. Therefore, the base fragility cumulative distribution function (CDF) model was adjusted to different steels used in a typical design and to meet the code specification of the material model used in LS-DYNA. The adjustment consisted of shifting the distribution by -8.3 % (Ref. D4.1.27, p. 93). Thus the initial fragility curve was shifted by 8.3 % to a lower value of minimum elongation. The fragility curves before and after the shift are shown in and tabulated in Table D1.1-1. 316L stainless steel might be used for construction of some canisters and casks, but the stress-strain curves would be similar.

Fragility Curve of Steel 304 Annealed

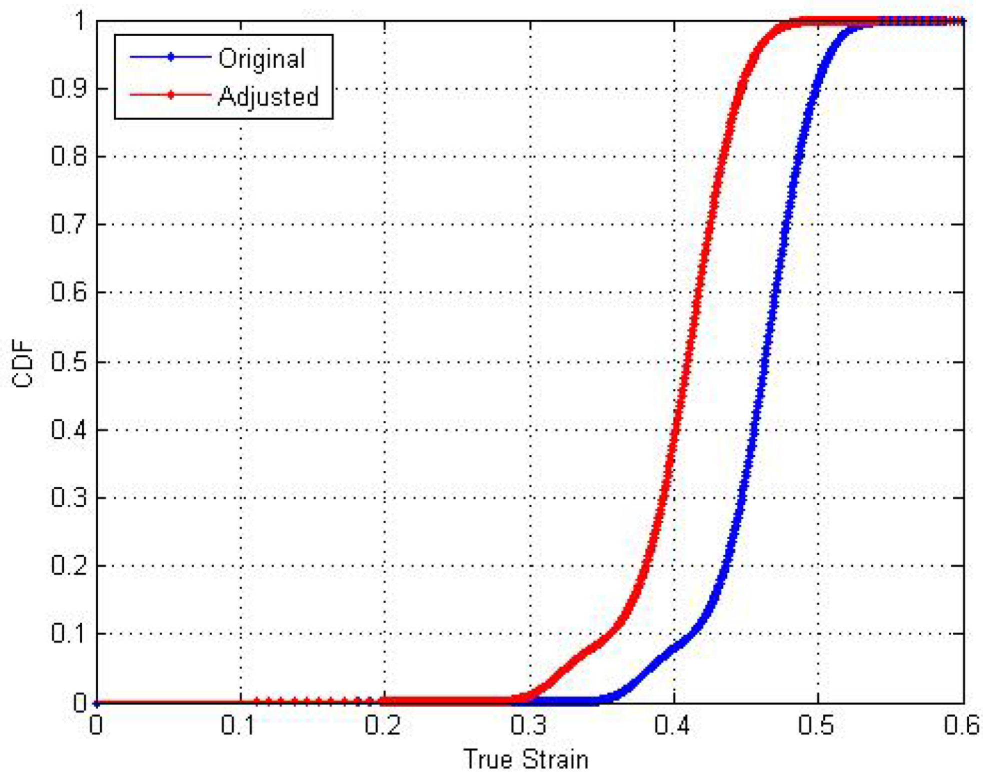

Source: Ref. D4.1.27, Figure 6.3.7-3

Figure D1.1-1. Original and Shifted Cumulative Distribution Functions (CDF) for Capacity (or Fragility) Plotted as a Function of True Strain

Table D1.1-1. Probability of Failure versus True Strain Tabulated for Figure D1.1-1

True Strain (*TS*)	$\frac{TS - TS_{mean}}{TS_{std}}$	Probability of Failure Original	Probability of Failure Adjusted (-8.3% shift)
0.00	-1.70	0.0000E+00	1.6754E-15
0.01	-1.65	2.0924E-16	1.8688E-15
0.02	-1.60	4.1848E-16	2.0622E-15
0.03	-1.55	6.2772E-16	2.2555E-15
0.04	-1.50	8.3696E-16	2.4489E-15
0.05	-1.45	1.0462E-15	2.6422E-15
0.06	-1.41	1.2554E-15	2.8356E-15
0.07	-1.36	1.4647E-15	3.0290E-15
0.08	-1.31	1.6739E-15	3.2223E-15
0.09	-1.26	1.8832E-15	3.4157E-15
0.10	-1.21	2.0924E-15	3.6090E-15
0.11	-1.16	2.3016E-15	3.8024E-15
0.12	-1.11	2.5109E-15	2.8601E-14
0.13	-1.07	2.7201E-15	2.3645E-13
0.14	-1.02	2.9294E-15	1.6225E-12
0.15	-0.97	3.1386E-15	9.7686E-12
0.16	-0.92	3.3478E-15	5.2952E-11
0.17	-0.87	3.5571E-15	2.6233E-10
0.18	-0.82	3.7663E-15	1.2513E-09
0.19	-0.78	2.1733E-14	6.9107E-09
0.20	-0.73	2.1209E-13	2.6769E-08
0.21	-0.68	1.7358E-12	1.1600E-07
0.22	-0.63	1.1373E-11	4.8126E-07
0.23	-0.58	6.4625E-11	1.9316E-06
0.24	-0.53	4.1126E-10	7.5246E-06
0.25	-0.48	2.4773E-09	2.8566E-05
0.26	-0.44	1.2132E-08	1.0566E-04
0.27	-0.39	5.2343E-08	3.7635E-04
0.28	-0.34	2.4478E-07	1.2625E-03
0.29	-0.29	1.0945E-06	3.8474E-03
0.30	-0.24	4.7123E-06	1.0185E-02
0.31	-0.19	1.9709E-05	2.2466E-02
0.32	-0.15	7.9860E-05	4.0237E-02
0.33	-0.10	3.1104E-04	5.9110E-02
0.34	-0.05	1.1366E-03	7.5125E-02
0.35	**0.00**	**3.7379E-03**	**8.9858E-02**
0.36	0.05	1.0506E-02	1.0973E-01
0.37	0.10	2.3978E-02	1.4282E-01
0.38	0.15	4.3259E-02	1.9679E-01
0.39	0.19	6.2863E-02	2.7687E-01
0.40	0.24	7.9100E-02	3.8310E-01
0.41	0.29	9.5539E-02	5.0814E-01
0.42	0.34	1.2068E-01	6.3823E-01
0.43	0.39	1.6410E-01	7.5736E-01
0.44	0.44	2.3393E-01	8.5309E-01
0.45	0.48	3.3371E-01	9.2036E-01
0.46	0.53	4.5893E-01	9.6161E-01
0.47	0.58	5.9615E-01	9.8363E-01
0.48	0.63	7.2682E-01	9.9385E-01
0.49	0.68	8.3454E-01	9.9797E-01
0.50	0.73	9.1117E-01	9.9941E-01
0.51	0.78	9.5806E-01	9.9985E-01
0.52	0.82	9.8270E-01	9.9997E-01
0.53	0.87	9.9379E-01	9.9999E-01
0.54	0.92	9.9807E-01	1.0000E+00
0.55	0.97	9.9948E-01	1.0000E+00
0.56	1.02	9.9988E-01	1.0000E+00
0.57	1.07	9.9998E-01	1.0000E+00
0.58	1.11	1.0000E+00	1.0000E+00
0.59	1.16	1.0000E+00	1.0000E+00
0.60	1.21	1.0000E+00	1.0000E+00
0.61	1.26	1.0000E+00	1.0000E+00
0.62	1.31	1.0000E+00	1.0000E+00
0.63	1.36	1.0000E+00	1.0000E+00
0.64	1.41	1.0000E+00	1.0000E+00
0.65	1.45	1.0000E+00	1.0000E+00
0.66	1.50	1.0000E+00	1.0000E+00
0.67	1.55	1.0000E+00	1.0000E+00
0.68	1.60	1.0000E+00	1.0000E+00
0.69	1.65	1.0000E+00	1.0000E+00
0.70	1.70	1.0000E+00	1.0000E+00

NOTE: The mean for true strain is 0.35, shown in bold. The standard deviation (std) of true strain is 0.21.

Source: Ref. D4.1.27, Table 6.3.7.3-1

The weldment, at best, can have the same mechanical properties as the hosting metal (native metal), but it is usually more brittle than the hosting metal. The failure likelihood of the weldment substructure was considered, reflecting weighting factors of both 1.0 and 0.75 applied to estimated true strain at failure.

The capacity function is based on coupon tensile strength tests in uniaxial tension. However, cracking of a stainless steel may not be determined simply by comparing the calculated plastic strain to the true strain of failure, because the equivalent (or effective) plastic strain (EPS) is calculated from a complex 3-D state of stress, while the true strain at failure was based on data from a 1-D state of stress. A 3-D state of stress may constrain plastic flow in the material and lower the EPS at which failure occurs. This loss of ductility is accounted for by the use of a triaxiality factor, which is the ratio of normal stress to shear stress on the octahedral plane, normalized to unity for simple tension. For the purpose of determining the probability of structural failure, LLNL (Ref. D4.1.27) set the ductility ratio to 0.5. This is equivalent to a triaxiality factor of 2, which corresponds to a state of biaxial tension.

Failure of containment can occur when strain in a component is of sufficient magnitude that it results in breakage or puncture of the container. The probability of failure is calculated based on the maximum strain for a single finite element brick obtained from LS-DYNA simulations. Fracture propagation takes place on the milliseconds time-scale and thus propagates across the canister wall thickness very quickly, compared to the time-frame of the LS-DYNA simulations. Furthermore, the fragility curve is obtained on the basis of a maximum average strain over the thickness of the respective specimens, which are 2 in. long stainless steel 304L specimens. Although LS-DYNA results provide multiple values of the strain through the thickness of the canister wall (the wall thickness being represented by multiple finite element layers), it is more conservative to use the maximum strain value at a single finite element brick than the average of the multiple values across the thickness of the wall.

The probability of failure for each impact scenario is evaluated by finding the maximum strain at a location in which a through-wall crack would constitute a radionuclide release. A probability of failure is determined from the CDF of capacity or fragility curve (as discussed below) from the global maximum strain.

A conservative approach and aid to computational efficiency is achieved by performing calculations focusing on the regions of the container having high strain (and deformation) after a drop ("hot zones"). An importance sampling strategy was used which places greater-than-random emphasis on ranges of input-variable values, and/or on combinations of such value ranges, that are more likely to affect output. This approach is an alternative to Monte Carlo methods with the important advantage that possible combinations of upper-bound variable values are in fact incorporated into each probabilistic estimate of expected model output (which is not always guaranteed by uniform sampling).

Using the general probabilistic approach summarized here, LLNL (Ref. D4.1.27) calculated failure probabilities for representative canisters in an aging overpack, and in a transportation cask, and for the representative canister itself, as presented in Tables D1.2-2 through D1.2-5. For the drop of a 10-metric-ton load onto a cask, the falling mass is modeled as a rigid (unyielding) wall, oriented normal to longitudinal axis of the cask.

D1.2 IDAHO NATIONAL LABORATORY ANALYSIS OF SPENT NUCLEAR FUEL CANISTERS AND MULTICANISTER OVERPACKS

Drop tests of prototype canisters conducted by the Idaho National Laboratory (INL) confirmed that the stainless steel shell material can undergo significant strains without material failure leading to loss of containment. These drop tests also validated analytical models used to predict strains under various drop scenarios. Table D1.2-6 shows scenarios selected to address potential drop scenarios at YMP facilities and the predicted strains.

INL performed FEA (using ABAQUS/Explicit, which, like LS-DYNA, has been used in nuclear facility and non-nuclear industrial applications, and is appropriate to model nonlinear, transient responses of a passive component to a structural challenge such as a drop or an impact) of 23-foot drops, three degrees off vertical, to determine the extent of strain at various positions in the bottom head, cylindrical shell, and joining weld. The strain was evaluated and reported for the inside, outside, and middle layers (Ref. D4.1.64). The DOE SNF canisters were modeled at 300°F, the maximum skin temperature expected due to the heat evolved by the fuel (based on review of thermal analyses performed by transportation casks vendors), resulting in diminished casing material strength. It was found that greater strains would be expected in the MCOs at ambient temperatures than at elevated temperatures.

During a canister drop event, the majority of the kinetic energy at impact performs work on the material, which causes the worst locations to exhibit plastic strain. A good measure of this work is equivalent plastic strain, which is a cumulative strain measure that takes into account the deformation history starting at impact. From the peak equivalent plastic strain, LLNL (Ref. D4.1.27) developed failure probabilities using the method described in Section D1.1 for an 18 in. and 24 in. DOE standard canister and an MCO. Results are summarized in Table D1.2-7.

Table D1.2-1. Container Configurations and Loading Conditions

Container	Configuration	Drop Type/Impact Condition[a]	Drop Height
AO (aging overpack) cell with canister inside	Representative canister inside AO	A IC 1: End with vertical orientation	3-ft vertical
		A IC 2: Slapdown from a vertical orientation and 2.5 mph horizontal velocity	0-ft vertical
Transportation cask with spent nuclear fuel (SNF) canister inside	Representative canister inside representative cask	T IC 1a: End, with 4 degree off-vertical orientation T.IC 1b: Same as T.IC 1a T.IC 1c: Same as T.IC 1a	12-ft vertical 13.1-ft vertical 30-ft vertical
		T IC 2a: End, with 4 degree off-vertical orientation, and approximated slapdown T.IC 2b: Same as T.IC 2a, with no free fall	13.1-ft vertical 0-ft vertical
		T IC 3: Side, with 3 degree off-horizontal orientation	6-ft vertical
		T IC 4: Drop of 10-metric-ton load onto top of cask	10-ft vertical
DPC (dual-purpose canister) TAD (transportation, aging, and disposal) canister	Representative canister	D IC 1a: End, with vertical orientation D IC 1b: Same as D.IC 1a	32.5-ft vertical 40-ft vertical
		D IC 2a: End, with 4 degree off-vertical orientation D IC 2b: Same as D.IC 2a D IC 2c: Same as D.IC 2a	23-ft vertical 10-ft vertical 5-ft vertical
		D IC 3: 40 ft/min horizontal collision inside the CTM bell	No drop
		D IC 4: Drop of 10-metric-ton load onto top of canister	10-ft vertical
		D.IC 2a: Hourglass-control study for end drop, with 4 degree off-vertical orientation	23-ft vertical
		D.IC 2a: Friction coefficient sensitivity study for end drop, with 4 degree off-vertical orientation	23-ft vertical
		D.IC 2a: Mesh density study for end drop, with 4 degree off-vertical orientation	23-ft vertical
		D.IC 2a: Shell- and bottom-lid-thickness sensitivity study for end drop, with 4 degree off-vertical orientation	23-ft vertical
DSNF (DOE spent nuclear fuel) canister	INL-analyzed case	O.IC 1: End, with 3-degree-off vertical orientation	23-ft vertical

NOTE: A = aging overpack; CTM = canister transfer machine; ft = foot; D = dual-purpose canister; IC = impact condition; INL = Idaho National Laboratory; min = minute; mph = miles per hour; O = DOE SNF canister; T = transportation cask.

Source: [a] Ref. D4.1.27, Table 4.3.3-1a

Table D1.2-2. Failure Probabilities with and without Triaxiality Factor, with and without the Fragility Curve Adjustment, for Representative Canister within an Aging Overpack

Container Type/ Impact Condition[a]	Impact Condition Description	Max EPS[b]	Failure Probability[b]			
			Original CDF Fragility Curve w/o Adjustment		CDF Fragility Curve Adjusted for Minimum Elongation (-8.3% Shift)	
			w/o Triaxiality	with Triaxiality	w/o Triaxiality	with Triaxiality
A.IC 1	3-ft end drop, with vertical orientation	0.16%	$<1 \times 10^{-8}$	$<1 \times 10^{-8}$	$<1 \times 10^{-8}$	$<1 \times 10^{-8}$
A.IC 2	Slapdown from a vertical orientation and 2.5-mph horizontal velocity	0.82%	$<1 \times 10^{-8}$	$<1 \times 10^{-8}$	$<1 \times 10^{-8}$	$<1 \times 10^{-8}$

NOTE: [a] "A" stands for aging overpack. "IC" stands for impact condition. Both are defined in Table D1.2-1.
[b] Values of Max EPS and failure probability are applicable to the SNF canister.
CDF = cumulative distribution function; EPS = equivalent (or effective) plastic strain.

Source: Ref. D4.1.27, Table 6.3.7.6-1

Table D1.2-3. Failure Probabilities with and without Triaxiality Factor, with and without Fragility Curve Adjustment, for Representative Canister

Container Type/ Impact Condition[a]	Impact Condition Description	Max EPS[b]	Failure Probability[b]: Original CDF Fragility Curve w/o Adjustment, w/o Triaxiality	Original CDF Fragility Curve w/o Adjustment, with Triaxiality	CDF Fragility Curve Adjusted for Minimum Elongation (-8.3% Shift), w/o Triaxiality	CDF Fragility Curve Adjusted for Minimum Elongation (-8.3% Shift), with Triaxiality
D.IC 1a	32.5-ft end drop, with vertical orientation	2.13%	$<1 \times 10^{-8}$	$<1 \times 10^{-8}$	$<1 \times 10^{-8}$	$<1 \times 10^{-8}$
D.IC 1b	40-ft end drop, with vertical orientation	2.65%	$<1 \times 10^{-8}$	$<1 \times 10^{-8}$	$<1 \times 10^{-8}$	$<1 \times 10^{-8}$
D.IC 2a	23-ft end drop, with 4-degree off-vertical orientation	24.19%	$<1 \times 10^{-8}$	**7.71×10^{-1}**	**9.72×10^{-6}**	**9.96×10^{-1}**
D.IC 2b	10-ft end drop, with 4-degree off-vertical orientation	19.71%	$<1 \times 10^{-8}$	**7.01×10^{-2}**	**1.73×10^{-8}**	**3.19×10^{-1}**
D.IC 2c	5-ft end drop, with 4-degree off-vertical orientation	15.76%	$<1 \times 10^{-8}$	**4.10×10^{-5}**	$<1 \times 10^{-8}$	**3.12×10^{-2}**
D.IC 3	40-ft/min horizontal side collision	0.16%	$<1 \times 10^{-8}$	$<1 \times 10^{-8}$	$<1 \times 10^{-8}$	$<1 \times 10^{-8}$
D.IC 4	10-ft drop of 10-metric-ton load onto top of canister	0.75%	$<1 \times 10^{-8}$	$<1 \times 10^{-8}$	$<1 \times 10^{-8}$	$<1 \times 10^{-8}$
D.IC 2a S1-L1	Same as D.IC 2a	24.19%	$<1 \times 10^{-8}$	**7.71×10^{-1}**	**9.72×10^{-6}**	**9.96×10^{-1}**
D.IC 2a S2-L1	Same as D.IC 2a	21.52%	$<1 \times 10^{-8}$	**1.66×10^{-1}**	**2.44×10^{-7}**	**7.62×10^{-1}**
D.IC 2a S3-L1	Same as D.IC 2a	16.53%	$<1 \times 10^{-8}$	**3.37×10^{-4}**	$<1 \times 10^{-8}$	**6.02×10^{-2}**
D.IC 2a S1-L2	Same as D.IC 2a	23.34%	$<1 \times 10^{-8}$	**5.52×10^{-1}**	**3.07×10^{-6}**	**9.78×10^{-1}**
D.IC 2a S1-L3	Same as D.IC 2a	25.15%	$<1 \times 10^{-8}$	**9.28×10^{-1}**	**3.48×10^{-5}**	**1.00**
D.IC 2a S2-L3	Same as D.IC 2a	22.57%	$<1 \times 10^{-8}$	**3.50×10^{-1}**	**1.07×10^{-6}**	**9.28×10^{-1}**
D.IC 2a S3-L3	Same as D.IC 2a	18.08%	$<1 \times 10^{-8}$	**1.22×10^{-2}**	$<1 \times 10^{-8}$	**1.14×10^{-1}**
D.IC 2a S2-L4	Same as D.IC 2a	24.07%	$<1 \times 10^{-8}$	**7.44×10^{-1}**	**8.27×10^{-6}**	**9.95×10^{-1}**
D.IC 2a S3-L4	Same as D.IC 2a	19.50%	$<1 \times 10^{-8}$	**6.29×10^{-2}**	**1.37×10^{-8}**	**2.77×10^{-1}**

NOTE: [a] "D" stands for dual-purpose canister. "IC" stands for impact condition. Both are defined in Table D1.2-1.

[b] Values of Max EPS and failure probability are applicable to the SNF canister. A range of canister shell and bottom plate thicknesses were evaluated. The values shown are for the configuration that yielded the highest strains (0.5-inch shell thickness and 2.313 inch bottom plate thickness)

See Table 6.3.3.5-1 of Ref. D4.1.27 for definitions of H1, F1, M1, etc. See Table 6.3.3.6-1 of Ref. D4.1.27 for definitions of S1, L1, etc.

CDF = cumulative distribution function; EPS = equivalent (or effective) plastic strain.

Source: Ref. D4.1.27, Table 6.3.7.6-3

Table D1.2-4. Failure Probabilities with and without Triaxiality Factor, with and without the Fragility Curve Adjustment, for the Representative Canister inside the Transportation Cask

Container Type/ Impact Condition[a]	Impact Condition Description	Max EPS[b]	Failure Probability[b]			
			Original CDF Fragility Curve w/o Adjustment		CDF Fragility Curve Adjusted for Minimum Elongation (-8.3% Shift)	
			w/o Triaxiality	with Triaxiality	w/o Triaxiality	with Triaxiality
T.IC 1a	12-ft end drop, with 4-degree off-vertical orientation	3.53%	$<1 \times 10^{-8}$	$<1 \times 10^{-8}$	$<1 \times 10^{-8}$	$<1 \times 10^{-8}$
T.IC 1b	13.1-ft end drop, with 4-degree off-vertical orientation	4.06%	$<1 \times 10^{-8}$	$<1 \times 10^{-8}$	$<1 \times 10^{-8}$	$<1 \times 10^{-8}$
T.IC 1c	30-ft end drop, with 4-degree off-vertical orientation	5.77%	$<1 \times 10^{-8}$	$<1 \times 10^{-8}$	$<1 \times 10^{-8}$	$<1 \times 10^{-8}$
T.IC 2a	13.1-ft end drop, with 4-degree off-vertical orientation, and approximated slapdown	4.35%	$<1 \times 10^{-8}$	$<1 \times 10^{-8}$	$<1 \times 10^{-8}$	$<1 \times 10^{-8}$
T.IC 2b	Approximated slapdown from vertical orientation	1.25%	$<1 \times 10^{-8}$	$<1 \times 10^{-8}$	$<1 \times 10^{-8}$	$<1 \times 10^{-8}$
T.IC 3	6-ft side drop, with 3-degree off-horizontal orientation	2.07%	$<1 \times 10^{-8}$	$<1 \times 10^{-8}$	$<1 \times 10^{-8}$	$<1 \times 10^{-8}$
T.IC 4	10-ft drop of 10-metric-ton load onto top of cask	0.96%	$<1 \times 10^{-8}$	$<1 \times 10^{-8}$	$<1 \times 10^{-8}$	$<1 \times 10^{-8}$
T.IC 5a	30-ft end drop, with vertical orientation	3.55%	$<1 \times 10^{-8}$	$<1 \times 10^{-8}$	$<1 \times 10^{-8}$	$<1 \times 10^{-8}$
T.IC 5b	30-ft end drop, with 4-degree off-vertical orientation	5.77%	$<1 \times 10^{-8}$	$<1 \times 10^{-8}$	$<1 \times 10^{-8}$	$<1 \times 10^{-8}$
T.IC 5c	30-ft end drop, with 45-degree off-vertical orientation	6.41%	$<1 \times 10^{-8}$	$<1 \times 10^{-8}$	$<1 \times 10^{-8}$	$<1 \times 10^{-8}$
T.IC 5d	30-ft end drop, with center of gravity over corner (i.e., point of impact)	6.63%	$<1 \times 10^{-8}$	$<1 \times 10^{-8}$	$<1 \times 10^{-8}$	$<1 \times 10^{-8}$

NOTE: [a] "T" stands for transportation cask. "IC" stands for impact condition. Both are defined in Table D1.2-1.
[b] Values of Max EPS and failure probability are applicable to the SNF canister.
CDF = cumulative distribution function; EPS = equivalent (or effective) plastic strain.

Source: Ref. D4.1.27, Table 6.3.7.6-2

Table D1.2-5. Failure Probabilities with and without Triaxiality Factor, with and without the Fragility Curve Adjustment, for the Transportation Cask

Container Type/ Impact Condition[a]	Impact Condition Description	Max EPS[b]	Failure Probability	
			CDF Fragility Curve Adjusted for Minimum Elongation (-8.3% Shift)	
			w/o Triaxiality	with Triaxiality
T.IC 1a	12-ft end drop, with 4-degree off-vertical orientation	9.20%	$<1 \times 10^{-8}$	$<1 \times 10^{-8}$
T.IC 1b	13.1-ft end drop, with 4-degree off-vertical orientation	9.37%	$<1 \times 10^{-8}$	$<1 \times 10^{-8}$
T.IC 1c	30-ft end drop, with 4-degree off-vertical orientation	11.25%	$<1 \times 10^{-8}$	9×10^{-7}
T.IC 2a	13.1-ft end drop, with 4-degree off-vertical orientation, and approximated slapdown	9.94%	$<1 \times 10^{-8}$	3×10^{-8}
T.IC 2b	Approximated slapdown from vertical orientation	5.30%	$<1 \times 10^{-8}$	$<1 \times 10^{-8}$
T.IC 3	6-ft side drop, with 3-degree off-horizontal orientation	7.42%	$<1 \times 10^{-8}$	$<1 \times 10^{-8}$
T.IC 4	10-ft drop of 10-metric-ton load onto top of cask	1.76%	$<1 \times 10^{-8}$	$<1 \times 10^{-8}$
T.IC 5a	30-ft end drop, with vertical orientation	3.17%	$<1 \times 10^{-8}$	$<1 \times 10^{-8}$
T.IC 5b	30-ft end drop, with 4-degree off-vertical orientation	11.25%	$<1 \times 10^{-8}$	9×10^{-7}
T.IC 5c	30-ft end drop, with 45-degree off-vertical orientation	70.56%	1	1
T.IC 5d	30-ft end drop, with center of gravity over corner (i.e., point of impact)	44.88%	0.9	1

NOTE: [a] "T" stands for transportation cask. "IC" stands for impact condition. Both are defined in Table D1.2-1.
[b] Values of Max EPS and failure probability are applicable to the structural body of the transportation cask, which excludes the shield and shield shell.
CDF = cumulative distribution function; EPS = equivalent (or effective) plastic strain.

Source: Probabilities calculated using Table D1.1-1 based on strains reported in Ref. D4.1.27, Table 6.3.7.6-2

Table D1.2-6. Strains at Various Canister Locations Due to Drops

Canister	Component	Maximum PEEQ Strains (%) Outside Surface	Mid-Surface	Inside Surface	Load Case/ Conditions
18-inch DOE STD canister	Lower head	8	3	6	300°F, 23-foot drop, 3 degrees off-vertical Material: ASME Code minimum strengths
	Lower head-to-main shell weld	2	2	3	
	Main shell	2	2	3	
	Upper head-to-main shell weld	0	0	0	
	Upper head	1	0.2	2	
24-inch DOE STD canister	Lower head	2	0.7	1	300°F, 23-foot drop, 3 degrees off-vertical Material: ASME Code minimum strengths
	Lower head-to-main shell weld	0.2	0.3	0.5	
	Main shell	0.2	0.3	0.5	
	Upper head-to-main shell weld	0	0	0	
	Upper Head	0	0	0	
MCO	Lower head	35	16	14	70°F, 23-foot drop, 3 degrees off-vertical Material: Actual material properties (significantly higher than ASME Code minimums)
	Lower head-to-main shell weld	21	11	11	
	Main shell	13	15	29	
	Upper head-to-main shell weld	0	0	0	
	Upper head	0	0	0	

NOTE: ASME = The American Society of Mechanical Engineers; DOE STD = U.S. Department of Energy standard; MCO = multicanister overpack; PEEQ = peak equivalent.

Source: Ref. D4.1.64, Tables 13, 14, and 16

Table D1.2-7. Failure Probabilities for the DOE Spent Nuclear Fuel (DSNF) Canisters and Multicanister Overpack (MCO)

Component	**Peak Equivalent Plastic Strain (%)**			**Probability of Failure**					
				Original CDF			**CDF adjusted to min elongation**		
	Outside Surface	**Middle**	**Inside Surface**	**Outside Surface**	**Middle**	**Inside Surface**	**Outside Surface**	**Middle**	**Inside Surface**
18-inch standard canister containment PEEQ strains, 3 degrees off vertical drop, 300°F									
Lower Head	8	3	6	<1E-08	<1E-08	<1E-08	<1E-08	<1E-08	<1E-08
Lower Head-to-Main Shell Weld	2	2	3	<1E-08	<1E-08	<1E-08	<1E-08	<1E-08	<1E-08
Main Shell	2	2	3	<1E-08	<1E-08	<1E-08	<1E-08	<1E-08	<1E-08
Upper Head-to-Main Shell Weld	0	0	0	<1E-08	<1E-08	<1E-08	<1E-08	<1E-08	<1E-08
Upper Head	1	0.2	2	<1E-08	<1E-08	<1E-08	<1E-08	<1E-08	<1E-08
24-inch standard canister containment PEEQ strains, 3 degrees off vertical drop, 300°F									
Lower Head	2	0.7	1	<1E-08	<1E-08	<1E-08	<1E-08	<1E-08	<1E-08
Lower Head-to-Main Shell Weld	0.2	0.3	0.5	<1E-08	<1E-08	<1E-08	<1E-08	<1E-08	<1E-08
Main Shell	0.2	0.3	0.5	<1E-08	<1E-08	<1E-08	<1E-08	<1E-08	<1E-08
Upper Head-to-Main Shell Weld	0	0	0	<1E-08	<1E-08	<1E-08	<1E-08	<1E-08	<1E-08
Upper Head	0	0	0	<1E-08	<1E-08	<1E-08	<1E-08	<1E-08	<1E-08
4 MCO containment PEEQ strains, 3 degrees off vertical drop, 70°F									
Bottom	35	16	14	3.74E-03	<1E-08	<1E-08	8.99E-02	<1E-08	<1E-08
Bottom-to-Main Shell	21	11	11	<1E-08	<1E-08	<1E-08	1.16E-07	<1E-08	<1E-08
Main Shell	13	15	29	<1E-08	<1E-08	1.09E-06	<1E-08	<1E-08	3.85E-03
Collar	0	0	0	<1E-08	<1E-08	<1E-08	<1E-08	<1E-08	<1E-08
Cover	0	0	0	<1E-08	<1E-08	<1E-08	<1E-08	<1E-08	<1E-08

NOTE: CDF = cumulative distribution function; DOE STD = U.S. Department of Energy standard; MCO = multicanister overpack; PEEQ = peak equivalent.

Source: Ref. D4.1.27, Tables 6.3.7.6-4 and 6.3.7.6-5

D1.3 PROBABILITIES OF FAILURE OF HIGH LEVEL WASTE CANISTERS DUE TO DROPS

The probability of failure for drops of HLW canisters was assessed by evaluating actual drop test data. Several series of tests were conducted including vertical, top, and corner drops of steel containers. The reports on these tests are summarized in *Leak Path Factors for Radionuclide Releases from Breached Confinement Barriers and Confinement Areas* (Ref. D4.1.17). No leaks were found after 27 tests, 14 of which were from 23 feet and 13 of which were from 30 feet. These tests can be interpreted as a series of Bernouilli trials, for which the outcome is the breach, or not, of the tested canister. The observation of zero failures in 13 tests was interpreted using a beta-binomial conjugate distribution Bayes analysis.

A uniform prior distribution, which indicates prior knowledge that the probability of failure is between 0 and 1, may be represented as a Beta(r,s) distribution in which both r and s equals 1. The conjugate pair likelihood function for a Beta(r,s) distribution is a Binomial(n, N) where n represents the number of failures within the tests and N represents the number of tests. The posterior distribution resulting from the conjugate pairing is also a Beta distribution with parameters r' and s', which are defined as follows (Equation D-1):

$$r' = r + n \quad \text{and} \quad s' = s + N - n \qquad \text{(Eq. D-1)}$$

The mean, μ, and standard deviation, σ, of the posterior distribution are determined using the following equations:

$$\mu = r' / (r' + s') \quad \text{and} \quad \sigma = \{r's' / [(r' + s' + 1)(r' + s')^2]\}^{1/2} \qquad \text{(Eq. D-2)}$$

For n = 0 and N = 13, Equation D-2 results in $\mu = 0.067$ and $\sigma = 0.062$. For n = 0 and N = 27, $\mu = 0.034$ and $\sigma = 0.033$. These values are used for the failure probability of a dropped HLW canister, for example during its transfer by a canister transfer machine.

One element of the Nuclear Safety Design Basis (Section 6.9) requires that the transportation cask, which will deliver HLW and DOE standardized canisters, be designed to preclude contact between the canister and a transportation cask lid or other heavy object that might fall. Similarly, other large heavy objects are precluded from damaging these canisters, when residing within a co-disposal waste package by the design of the waste package, which includes separator plates that extend well above the canisters. These scenarios are not quantitatively analyzed herein.

The combined INL and LLNL analyses discussed previously conclude that a DOE SNF canister has a probability of breach less than 1E-08 for a 23-foot drop, 4 degrees off-normal (i.e., 4 degrees from vertical) onto an unyielding rigid surface. The LLNL results demonstrate that generally strains from impact and probability of failure is higher for off-normal drops than normal (i.e., vertical) drops for the same height. The LLNL results further show that a 10-ton load dropped from 10 feet onto a representative canister also results in a probability of breach of less than 1E-08. *Qualitative Analysis of the Standardized DOE SNF Canister for Specific Canister-on-Canister Drop Events at the Repository*. EDF-NSNF-087 (Ref. D4.1.67) states that canister integrity was maintained for a 30-foot drop test onto a rigid, unyielding surface. The report discusses drop of a HLW canister on a DOE SNF canister and drop of a DOE SNF canister onto another one. Drops of these canisters onto canisters in the Initial Handling Facility (IHF) or Canister Receipt and Closure Facility (CRCF) would occur with drop heights of less than 10 feet. Two main differences are noted between a drop of a DOE SNF and a drop of a HLW canister onto a DOE SNF. The first is that substantially lower kinetic energy of impact of the latter drop would result in significantly less skirt deformation. The non-flat bottom nature of the HLW/DOE SNF interaction would have a different skirt deformation pattern that the flat bottomed drop. INL concludes that the skirt would be expected to absorb the bulk of the heaviest HLW canister (4.6 tons) drop energy and DOE SNF canister integrity would be maintained. A difference between a 10-ton drop of a load onto a representative canister and a drop onto a DOE SNF canister results from the difference diameters of the target as well as different materials and lid thicknesses. Nevertheless, INL concludes that the impact from 10 feet of a HLW canister onto a DOE SNF canister is less challenging than impact from a 30-foot drop. Since the probability from a 23-foot drop was calculated to be less than 1E-08, it is conservative to use a value of 1E-05 for the probability of failure of an HLW on DOE SNF impact. The increased value is assigned to account for uncertainties owing to the differences noted above.

D1.4 PROBABILITIES OF FAILURE OF WASTE PACKAGES DUE TO DROPS AND IMPACTS

The probabilities of containment failure are evaluated by comparing the challenge load with the capacity of the waste package to withstand that challenge in a manner similar to that described in *Interim Staff Guidance HLWRS-ISG-02, Preclosure Safety Analysis - Level of Information and Reliability Estimation.* HLWRS-ISG-02 (Ref. D4.1.56), and summarized in Section 4.3.2.2. Three scenarios are evaluated for the potential loss of containment by waste packages due to drops and impacts:

- Two-foot horizontal drop
- 3.4 mph end-to-end impact
- Rockfall on waste package in subsurface tunnels.

An additional scenario, drop of a waste package shield ring onto a waste package, is considered in Section D1.4.4.

For this assessment, the potential load has been determined by FEA in the calculations cited below as the sources of inputs. The load is expressed in terms of stress intensities and as expended toughness fraction (ETF), which is the ratio of the stress intensity to the true tensile strength. The ETF is used to obtain the failure probability by the following (Equation D-3):

$$P = \int_{-\infty}^{x} N(t)\,dt \quad and \quad x = \frac{ETF - 1}{COV} \qquad \text{(Eq. D-3)}$$

where

P	=	probability of failure
N(t)	=	standard normal distribution with mean of zero and standard deviation of one
T	=	variable of integration
ETF	=	expended toughness fraction
COV	=	coefficient of variation = ratio of standard deviation to mean for strain capacity distribution, applied here to stress capacity or true tensile strength

The capacity is the true tensile strength of the material, the stress the material can withstand before it separates. The minimum true tensile strength, σ_u, for the Alloy 22 typically used for the outer corrosion barrier (OCB) of the waste package is 971 MPa (Ref. D4.1.20, Section 7.7, p. 162). The variability in the capacity is expressed as the standard deviation of a normal distribution that includes strength variation data and variability of the toughness index, I_T, computed without triaxialty adjustments (uniaxial test data). The standard deviation as percent of the mean of σ_u is 7.3 % (Ref. D4.1.20, Section 7.6, p. 162). The distribution of elongations used for defining the fragility curve in the LLNL analysis was expressed as two normal distributions, the larger of which was with a mean of 59.3 % elongation and a standard distribution of 4.22 % elongation, or a coefficient of variation (COV) of 0.0712 (Ref. D4.1.27, Section 6.3.7.3). Thus the 0.073 reported for the OCB material is conservative compared with the LLNL data and is used for the COV in the expression above. The possibility of waste package weld defects is not explicitly considered in the analysis. However, as noted in Section D.1.4.5, weld defects are not expected to contribute significantly to the probability of waste package failure due to drops or other impacts.

D1.4.1 Waste Package Drop

A study investigating the structural response of the naval long waste package to a drop while it is being carried on the emplacement pallet, found the ETF for the OCB to be 0.29 for a 10 m/sec flat impact (Ref. D4.1.20, Table 7-15, pg. 117), equivalent to a 16.7-foot drop. This corresponds to a failure probability of less than 1×10^{-8}. The failure of the OCB is used to define the loss of containment, taking no credit for the inner vessel and the canister within. The description of the transport and emplacement vehicle (TEV) provided in *Mechanical Handling Design Report: Waste Package Transport and Emplacement Vehicle* (Ref. D4.1.12) mentions that the floor plate is lifted by four jacks and guided by a roller. The guide roller precludes tilted drops of the flat bed of the TEV. As was done for the results from LLNL, to introduce an additional measure of conservatism, a failure probability of 1×10^{-5} is used for the probability that the waste package containment would fail due to a two-foot horizontal drop, which is much less severe than the modeled 16.7-foot drop.

D1.4.2 Rockfall onto a Waste Package

A seismic event during the preclosure period could cause rocks to fall from the ceiling of a drift onto the waste packages stored there prior to deployment of the drip shields. The extent of damage has been predicted for several levels of impact energy of falling rocks (Ref. D4.1.26). The maximum credible impact energy from a falling rock is about 1×10^6 joules (J) (Ref. D4.1.21, p. 57). The maximum ETF resulting from rockfall impacting with approximately 1×10^6 J is about 0.11 (Ref. D4.1.26, p. 54, Table 5), corresponding to a failure probability less than 1×10^{-8}. As was done for the results from LLNL, to introduce an additional measure of conservatism, a failure probability of 1×10^{-5} should be used for the probability that the waste package containment would fail due to rockfall on the waste package.

D1.4.3 Results for the Three Assessed Scenarios

The failure probabilities for the three scenarios, derived from the results in the cited reports, are summarized in Table D1.4-1.

Table D1.4-1. Waste Package Probabilities of Failure for Various Drop and Impact Events

Event	Probability of Failure
2-Foot Horizontal Drop	$< 1 \times 10^{-5}$
3.4 mph end-to-end impact	$< 1 \times 10^{-5}$
20 metric ton Rockfall on Waste Package with and without Rock Bolt[a] Impacting the Waste Package	$< 1 \times 10^{-5}$

NOTE: [a] A rock bolt is a long anchor bolt, for stabilizing rock excavations, which may be tunnels or rock cuts.

Source: Original

D1.4.4 Drop of a Waste Package Shield Ring onto a Waste Package

After the co-disposal waste package has been welded closed in the Waste Package Positioning Room, the shield ring is lifted from it before the waste package transfer trolley is moved into the load out area. Grapple failures might cause the drop to occur at a variety of orientations relative to the top of the waste package. A frequency of canister breach from a potential drop as high as 10 feet is considered here. For a canister breach to occur, the shield ring must penetrate the 1-inch thick outer lid made of SB 575 (Alloy 22) and the 9 inch thick stainless steel inner lid (SA 240) before having an opportunity to impact the canister (Ref. D4.1.13). There are six inches separating the inner and outer lids. In the radial center area of that space, which would be directly above the DOE SNF canister, is a stainless steel lifting device attached to the inner lid. This adds another layer of energy absorption.

The shield ring weighs approximately 15 tons and is made of stainless steel with a lighter weight neutron absorber material. The impact energy of a 15-ton shield ring dropping 10 feet would be 0.4 MJ (megajoule). The frequency of penetration of the sides of a waste package from a 20 metric ton rock impacting the side of the waste package with impact energy of 1 MJ is less than 1×10^{-8} (Table D1.4-1). The sides of a waste package are approximately three inches thick compared to a cumulative thickness (excluding lifting fixture) of 10 inches at the top. Although the impact energy could be more focused, the impact energy for the shield ring against the top of the waste package is less than the impact energy of the rockfall against the side and the top is much thicker than the side. The probability of failure due to shield ring impact against the top of the waste package is expected to be no worse than for the impact of a rock against the side. A conservative value of 1×10^{-5} is used in the analysis for this probability.

D1.4.5 Waste Package Weld Defects

Waste package closure involves engaging and welding the inner lid spread ring, inerting the waste package with helium, setting and welding the outer lid to the outer corrosion barrier, performing leak testing on the inner vessel closure, performing nondestructive examination of welds, and conducting postweld stress mitigation on the outer lid closure weld.

The weld process of the waste package closure subsystem is controlled as a special process by the Quality Assurance Program (Ref. D4.1.29, Section 9.0). The activities performed by the system are controlled by approved procedures.

The principal components of the system include welding equipment; nondestructive examination equipment for visual, eddy current, and ultrasonic inspections of the welds and leak detection; stress mitigation equipment for treatment of the outer lid weld; inerting equipment; and associated robotic arms. Other equipment includes the spread ring expander tool, leak detection tools, cameras, and the remote handling system. The system performs its functions through remote operation of the system components.

The capability of the waste package closure subsystem will be confirmed by demonstration testing of a full-scale prototype system. The prototype includes welding, nondestructive examinations, inerting, stress mitigation, material handling, and process controls subsystems. The objective of the waste package closure subsystem prototype program is to design, develop, and construct the complete system required to successfully close the waste package. An iterative process of revising and modifying the waste package closure subsystem prototype will be part of the design process. When prototype construction is finalized, a demonstration test of the closure operations will be performed on only the closure end of the waste package; thus, the mock-up will be full diameter but not full height as compared to the waste package. The purpose of the demonstration test is to verify that the individual subsystems and integrated system function in accordance with the design requirements and to establish closure operations procedures. This program is coordinated with the waste package prototype fabrication program.

The principal functions of the waste package closure subsystem are to:

- Perform a seal weld between the spread ring and the inner lid, the spread ring and the inner vessel, and the spread ring ends; perform a seal weld between the purge port cap and the inner lid; and perform a narrow groove weld between the outer lid and the outer corrosion barrier.
- Perform nondestructive examination of the welds to verify the integrity of the welds and repair any minor weld defects found.
- Purge and fill the waste package inner vessel with helium gas to inert the environment.

- Perform a leak detection test of the inner lid seals to ensure the integrity of the helium environment in the inner vessel.

- Perform stress mitigation of the outer lid groove closure weld to induce compressive residual stresses.

The gas tungsten arc welding process is used for waste package closure welds and weld repairs. Welding is performed in accordance with procedures qualified to the *2001 ASME Boiler and Pressure Vessel Code* (Ref. D4.1.5, Section IX), as noted below:

- The spread ring and purge port cap welds are two-pass seal welds.
- The outer lid weld is a multipass full-thickness groove weld.

Welding process procedures will be developed that identify the required welding parameters. The process procedures will:

- Identify the parameters necessary to consistently achieve acceptable welds.
- State the control method for each weld parameter and the acceptable range of values.

The welds are inspected in accordance with examination procedures developed using *2001 ASME Boiler and Pressure Vessel Code* (Ref. D4.1.5, Section V and Section III, Division 1, Subsection NC) as a guide, with modification as appropriate:

- Seal welds—visual inspection
- Groove welds—visual, eddy current, and ultrasonic inspection.

A weld dressing end effector is used for weld repairs. The defect is removed, resulting in an excavated cavity of a predetermined contour. The excavated cavity surface is inspected using the eddy current inspection end effectors. Then the cavity is welded and inspected in accordance with the welding and inspection procedures.

The stress mitigation process for the outer lid closure weld is controlled plasticity burnishing. Controlled plasticity burnishing is a patented method of controlled burnishing to develop specifically tailored compressive residual stress with associated controlled amounts of cold work at the outer surface of the waste package outer lid closure weld.

The inner vessel of the waste package is evacuated and backfilled with helium through a purge port on the inner lid. The inerting process is in accordance with the inerting process described in NUREG-1536 (Ref. D4.1.54, Sections 8.0 and V.1). After the waste package inner vessel is backfilled by helium, both the spread ring welds and the purge port plug are leak tested in accordance with *2001 ASME Boiler and Pressure Vessel Code* (Ref. D4.1.5, Section V, Article 10, Appendix IX) to verify that no leakage can be detected that exceeds the rate of 10^{-6} std cm^3/sec.

Waste package closure welding, nondestructive examination, stress mitigation, and inerting are conducted in accordance with approved administrative controls. The processes for waste package closure welding, nondestructive examination, stress mitigation, and inerting will be developed in accordance with the codes and standards identified below. The processes are monitored by qualified operators, and resulting process data are checked and verified as acceptable by qualified individuals.

Waste package closure welding, nondestructive examination, stress mitigation, and inerting normal operating procedures will specify, for example, the welding procedure specification, nondestructive examination procedure, qualification and proficiency requirements for operators and inspectors, and acceptance and independent verification records for critical process steps.

The waste package closure subsystem–related welds, weld repairs, and inspections are performed in accordance with *2001 ASME Boiler and Pressure Vessel Code* (Ref. D4.1.5, Section II, Part C; Section III, Division I, Subsection NC; Section IX; Section V).

The inerting of the waste package is performed in accordance with the applicable sections of NUREG-1536 (Ref. D4.1.54).

PCSA event sequences involving waste packages include challenges ranging from low velocity collisions to a 20 metric ton rockfall to a spectrum of fires. Waste package failure probabilities are calculated to be very low. Furthermore, a significant conservatism in the analysis is that the containment associated with the canister is not included in the probability of containment breach. In other words, if the waste package breaches, radionuclide release is analyzed as if the canister has breached (if the event sequence is in Category 1 or Category 2). Analytically, the canister is not relied upon for event sequences involving waste packages. The analytical results from the LLNL analysis show a significant reduction in canister strains is achieved by transportation cask and aging overpack protection. Although not analyzed, a similar ameliorating effect on the canister would be expected to be provided by the waste package.

The weld, inspection and repair process ensures no significant defects to a high reliability. The event sequence analysis shows that all event sequences associated with waste package breach are Beyond Category 2. In the context of the event sequence analysis, a significant defect is one that would have increased the probability of breach of the canister within the waste package by orders of magnitude. Even for significant weld defects, the protection offered by the waste package to the canister containment function would remain. Therefore, the effect of waste package weld failure on loss of canister containment during event sequences is not further considered.

D1.4.6 Waste Package End-to-End Impact

An oblique impact of a long naval SNF waste package inside a TEV was modeled to assess the structural response (Ref. D4.1.19). Most of the runs were with initial impact velocity of 3.859 m/sec corresponding to a drop height of 0.759 m (2.49 ft). The maximum ETF for the 3.859 m/sec (12.66 ft/sec) oblique impact in the OCB is about 0.7 (Ref. D4.1.19, page 37, Table 7-3, runs 1, 2, and 3), corresponding to a failure probability of about 2×10^{-5}. The oblique impact should be bounding for a direct end impact Using Equation D-4, an ETF of 0.11 is estimated for the hypothesized 3.4 mph end-to-end collision (two TEVs each traveling 1.7 mph), corresponding to a failure probability of less than 1×10^{-8}. The failure of the OCB is used to define the loss of containment, taking no credit for the inner vessel and the canister within. As was done for the results from LLNL, to introduce an additional measure of conservatism, a failure probability of 1×10^{-5} is used for the probability that the waste package containment would fail due to a 3.4 mph end-to-end impact.

D1.5 PREDICTING OUTCOMES OF OTHER SITUATIONS BY EXTRAPOLATING STRAINS FOR MODELED SCENARIOS

Equation 17 in Section 6.3.2.2 demonstrates use of the probability of failure at a given drop height together with the COV to predict probabilities at other drop heights. A similar approach can be used to extrapolate from one strain to another to find the corresponding failure probability. The work done on damaging the container expressed in the form of strain should be roughly proportional to the energy input to the material due to the impact. The impact energy is proportional to the drop height or to the square of the impact velocity. Finite element modeling demonstrated that the increase in strain is actually less than proportional to increase in drop height (Ref. D4.1.27, Tables D1.2-3 and D1.2-4), so increasing the strain proportionally with drop height or the square of impact velocity is conservative. The strain is extrapolated by multiplying it by the square of the ratio of the velocity of interest to the reference velocity.

$$\tau_i = \tau_{ref}\left(\frac{v_i}{v_{ref}}\right)^2 \qquad \text{(Eq. D-4)}$$

where

τ_i	=	strain at velocity of interest (dimensionless)
τ_{ref}	=	strain at reference velocity (dimensionless)
v_i	=	velocity of interest (same units as v_{ref})
v_{ref}	=	reference velocity (same units as v_i)

In case D.IC.3, a 0.16 % strain (τ_{ref}) was predicted for a side impact of 40 ft/min (v_{ref}). Using Equation D-4 to extrapolate for an impact velocity of 2.5 miles/hr gives an estimated strain of 4.84 %.

The estimated strain is then compared with the fragility curve tabulated in D1.1-1. A failure rate of less than 1×10^{-8} is predicted for a strain of 4.84 %. Probabilities of failure for a range of impact velocities are listed in Table D1.5-1.

Table D1.5-1. Calculated Strains and Failure Probabilities for Given Side Impact Velocities

Impact Velocity			
(ft/sec)	(ft/min)	% strain	Probability of failure
0.67	40	0.16	$< 1\times 10^{-8}$
1	60	0.36	$< 1\times 10^{-8}$
2	120	1.44	$< 1\times 10^{-8}$
4	240	5.76	$< 1\times 10^{-8}$
6	360	13	$< 1\times 10^{-8}$
8	480	23	$< 1\times 10^{-5}$

NOTE: ft/min = feet per minute; ft/sec = feet per second.

Source: Original

A similar approach is applied to estimate failure probabilities for vertical drops greater than 40 feet. The strains are extrapolated using the ratio of drop heights rather than the squared ratio of impact velocities in Equation D-4.

For the DPC, the maximum EPS is 2.65 % for a 40-foot end drop (case D.IC.1b in Table D1.2-3). Strains of 2.98 % and 3.31 % are estimated for 45- and 50-foot drops, respectively. Doubling the strains to account for triaxiality and comparing these strains with Table D1.1-1 shows the probabilities of failure are both $< 1 \times 10^{-8}$. As before, conservative probabilities of 1×10^{-5} are used in the event sequence quantification.

For the DOE standard canister the maximum strain is 8 % in the lower head of the 18-inch canister resulting from a 23-foot drop 3 degrees off vertical (Table D1.2-6). By the same approach as above, 10.4 %, 15.7 %, and 17.4 % strains are estimated for 30-foot, 45-foot, and 50-foot drops. Doubling these strains and comparing with Table D1.1-1 yields the failure probabilities of 1×10^{-7}, 3×10^{-2}, and 9×10^{-2} for the 30-foot, 45-foot, and 50-foot drops, respectively. A conservative probability of 1×10^{-5} is used for the 30-foot drop of the DOE standardized canister.

D1.6 MISCELLANEOUS SCENARIOS

D1.6.1 Localized Side Impact on a Transportation Cask

One of the requirements specified for transportation casks is they be robust enough to survive a 40-inch horizontal drop onto an unyielding 6-inch diameter upright cylinder (Ref. D4.2.2, Paragraph 71.73). The impact energy for such a scenario involving a 250,000 pound cask (a typical weight for a loaded cask) – the Nuclear Assurance Corporation (NAC) STC has a loaded weight of 260,000 pounds (Ref. D4.1.50, p. 1.1-1) is about 1.1 MJ. The maximum weight of a forklift is considerably less than 20,000 kg. At a maximum speed of 2.5 mph (1.12 m/sec), the maximum impact energy would be 12.5 kJ (kilojoule), a factor of 90 less than the impact energy for the 40-inch drop of the cask. If the resultant strain is proportional to the impact energy and the drop event in the Safety Analysis Report (SAR) is just below the failure threshold (i.e., the median impact energy for failure), the impact energy due to the 2.5 mph impact would be a maximum of $1/90^{th}$ of the median failure impact energy, or 1 – 1/90 COVs less than a normalized median of 1. Equation D-3 is applicable substituting the ratio of impact energy to median failure impact energy for the factor ETF. Using 1/90 (=0.011) in place of the ETF in Equation D-3 gives a probability of failure of much less than 1×10^{-8} due to impact of a forklift against a transportation cask. If the impact speed were 9 mph instead of 2.5 mph, the impact energy would be about 1/7th of the energy in the SAR drop event, 0.14 would be used in place of the ETF in Equation D-3, and the probability of failure would still be less than 1×10^{-8}.

D1.6.2 Screening Argument for TAD Weld Defects

TAD canister closure is the process that closes the loaded TAD canister by welding the shield plug and fully draining and drying the TAD canister interior, followed by backfilling the TAD canister with helium and fully welding the TAD canister lid around its circumference onto the body of the TAD canister.

The process control program for the closure welds produced by the TAD canister closure system is controlled as a special process by the Quality Assurance Program (Ref. D4.1.29, Section 9.0).

TAD canister closure is done at the TAD canister closure station in the Cask Preparation Area. The shielded transfer cask containing a loaded TAD canister is transferred from the pool to the TAD canister closure station using the cask handling crane. The shielded transfer cask lid is unbolted and then removed using the TAD canister closure jib crane. The TAD canister is then partially drained via the siphon port in order to lower the water level below the shield plug in preparation for welding. The TAD canister welding machine is positioned onto the TAD canister shield plug using the TAD canister closure jib crane, and the shield plug is welded in place. After a weld is completed, visual examination of the weld is performed in addition to the eddy current testing and ultrasonic testing that are performed by the TAD canister welding machine.

A draining, drying, and inerting system is connected to the siphon and vent ports in the shield plug and used to dry the interior of the TAD canister, followed by backfilling it with helium gas. Port covers are then placed over the siphon and vent ports and welded in place using the TAD canister welding machine. The TAD canister welding machine is removed, and the outer lid is placed onto the TAD canister using the TAD canister closure jib crane. The TAD canister welding machine is positioned onto the TAD canister outer lid, and the lid is welded in place. The TAD canister welding machine is removed, and the shielded transfer cask lid is placed onto the shielded transfer cask using the TAD canister closure jib crane and installed. Hoses are connected to the fill and drain ports on the shielded transfer cask, and the water is sampled for contamination. If the water is clean, the ports are opened to drain the annulus between the TAD canister and the shielded transfer cask. If the water is contaminated, then the annulus is flushed with treated borated water as needed. A drying system is then used to dry the annulus. The potential for contamination is kept to a minimum by the use of the inflatable seal.

The qualification of the TAD canister final closure welds is in accordance with ISG-18 (Ref. D4.1.55) as specified in *Basis of Design for the TAD Canister-Based Repository Design Concept* (Ref. D4.1.15, Section 33.2.2.36). Adherence to this guidance is deemed to provide reasonable assurance that weld defects occur at a low rate. However, TAD canister weld cracks are considered an initiating event after the TAD canister welding process in the Wet Handling

Facility (WHF). If this occurs, the radionuclide release would be minimal because the incoming casks and canisters have already been opened. After TAD canisters are welded, they are placed in aging overpacks and moved by the site transporter to the CRCF. The probability of TAD canister failure during removal from the aging overpack handling in the CRCF and placement into a waste package is considered in the CRCF event sequence analysis. The conditional probability of TAD canister failures during handling in the CRCF has been shown to be small. The low probability of weld defects and their size would not alter this result. After the TAD canister is placed in the waste package, the containment is considered to be the waste package and the TAD canister is no longer relied upon in event sequences involving mechanical impacts.

D2 PASSIVE FAILURE DUE TO FIRE

A risk assessment must consider a range of fires that can occur, as well as variations in the dynamics of the heat transfer and uncertainties in the failure temperature of the target. This section presents an analysis to determine the probability that a waste container will lose containment integrity or lose shielding in a fire. Section D2.1 addresses loss of containment and Section D2.2 addresses loss of shielding.

D2.1 ANALYSIS OF CANISTER FAILURE DUE TO FIRE

A common approach to safety analysis in regards to the effect of a fire is to postulate a specific fire (in terms of duration, combustible loading, heat rate, and other fire parameters) and then apply it to a specific configuration of a target. Then, a simple comparison is made between the temperature that the target reaches as a result of the fire, and the failure temperature of the target. Based on this comparison, a conclusion is made that either the target always fails, or never fails, or fails at some specific time. While such an approach may be appropriate for demonstrating that a specific design code has been met, it is not appropriate for a risk informed PCSA.

There are two parts to the assessment of the canister failure probability (sometimes referred to as the canister *fragility*): determining the thermal response of the canister to the fire and determining the temperature at which the canister will fail. In calculating the thermal response of the canister, variations in the intensity and duration of the fire are considered along with conditions that control the rate of heat transfer to the container (e.g., convective heat transfer coefficients, view factors, emissivities). In calculating the failure temperature of the canister, variations in the material properties of the canister material are considered along with variations in the loads that lead to failure.

D2.1.1 Uncertainty in Fire Severity

In the fragility analysis, fire severity is characterized by the fire temperature and duration, since these factors control the amount of energy that the fire could transfer to a target cask or canister. Uncertainty distributions were developed for the fire temperature and fire duration based on a review of generic and YMP-specific information.

D2.1.1.1 Uncertainty in Fire Duration

In the context of this study, this duration of the fire is from the perspective of the target (i.e., the cask or canister that could be compromised by the fire). Therefore, the fire duration used in the analysis is the amount of time a particular container is exposed to the fire, and not necessarily the amount of time a fire burns. As an example, a fire that propagates through a building over a four-hour period is not a four-hour hazard to a particular target. In calculating the exposure time for a specific target, it does not matter whether the fire started in the room where the target is, or it started in another room and ended where the target is, or the fire passed through the target room between its beginning and end. The exposure duration is how long the fire burns while consuming combustibles in the vicinity of the target. This allows a single probability distribution to be developed for the fire duration, regardless of how the fire arrived at the target, based on estimates of the duration of typical single-room fires.

In order to develop this curve, data on typical fire durations is required. A number of sources were used to derive insights regarding the range of expected durations of typical fires. The following sources were used:

- NUREG/CR-4679 (Ref. D4.1.53) reviewed the results of fire tests conducted by a number of organizations on a variety of types and amounts of combustible materials. Although focused on nuclear power plants, the materials assessed are typical of those found at a variety of industrial facilities.

- NUREG/CR-4680 (Ref. D4.1.52) reports on the results of a series of tests conducted by Sandia National Laboratories using a series of fuel source packages representative of trash found around nuclear power plants. Once again, these packages are typical of what might be found around other types of industrial facilities.

The tests were not extensive, and represented only particular configurations. In general, the fire durations were found to depend upon the amount, type, and configuration of the available combustible material.

Based on a review of the available information, it was determined that two separate uncertainty distributions (i.e., probability distributions that represent uncertainty) would be needed: one for conditions without automatic suppression and one for conditions with automatic suppression. The derivation of these two distributions is discussed below.

D2.1.1.2 Fire Duration without Automatic Fire Suppression

The first uncertainty distribution was developed for fires in which automatic fire suppression is not available. The vast majority of the tests conducted were for this case. The following summarizes information presented in the three references listed above.

Sandia National Laboratories conducted two large-scale cable fire tests using an initial fire source of five gallons of heptane fuel, and an additional fuel loading of two vertical cable trays with a 12.5 % fill consisting of 43 10-foot lengths of cable per tray (Ref. D4.1.53, Section 2.2.1). The only difference between the tests was that one test used unqualified cable and the other used IEEE-383 qualified cable. In the unqualified cable test, the cables reached peak heat release at approximately four minutes, and the rate decayed toward reaching zero at approximately 17 minutes. In the qualified cable test, the cables reached peak heat release at approximately seven minutes, and the rate decayed toward reaching zero at approximately 16 minutes.

Factory Mutual Research Corporation conducted tests for large-scale configurations of cable trays (Ref. D4.1.53, Section 2.2.3). One set of tests involved a configuration of 12 fully loaded horizontal trays in two stacked tiers. NUREG/CR-4679 (Ref. D4.1.53) provides detailed results for three of the "free-burn" tests (no automatic fire suppression). The first test reached and maintained the peak heat release rate at six minutes to 20 minutes, and reached zero at 25 minutes. The second test reached and maintained the peak heat release rate at seven minutes to 25 minutes, and reached zero at 34 minutes. The third test reached and maintained the peak heat release rate at 26 minutes to 40 minutes, and reached zero at 60 minutes.

Lawrence Berkeley Laboratory conducted tests on electrical cabinets (Ref. D4.1.53, Section 2.2.5). Two tests were conducted. The first was a single cabinet with only thermocouple wire and leads and no internal cabinet fuel loading. The fire that exposed the cabinet was two trash bags with loosely packed paper in a 32-gallon polyethylene trash receptacle, plus two cardboard boxes of packing "peanuts." This fire reached a peak heat release rate at seven minutes, and reached zero at 19 minutes. The second test involved two cabinets separated by a steel barrier. The cabinets contained a total of 64 lengths of cable (48 and 16). The source fire in this test was similar in nature to the first test, but had a heavier container and loose paper instead of the "peanuts." This fire had two peaks, at six minutes and 18 minutes, with the second being much larger than the first. The fire decayed toward reaching zero between 25 minutes and 30 minutes.

The Department of Health and Human Services sponsored a series of tests on various types of furnishing materials (Ref. D4.1.53, Section 3). While the specific types of furnishings are unlikely to be found in a YMP preclosure facility, these results are instructive for combinations of combustible materials that could be found. The first test was on a molded fiberglass chair with a metal frame. The fire reached a peak heat release rate in two minutes, and reached zero at 10 minutes. The second test was for a wood frame chair with latex foam cushions. This fire reached a peak heat release rate in four minutes and reached zero at 40 minutes. The final test was on four stackable, metal frame chairs with cushions that appeared to consist of a wood base, foam core, and vinyl cover. The fire reached a relatively steady state peak heat release rate from four minutes to 23 minutes, and reached zero at 38 minutes.

Sandia National Laboratories performed a series of nine tests on representative transient fuel fires (Ref. D4.1.52). Five different fuel packages were used for the tests. The first two fuel packages used mixed wastes representative of cleaning materials that might be left by maintenance personnel during routine operations. The first package was about 1.8 kg, and the second about 2.2 kg. The other difference between the two packages was the first package had more cardboard, whereas the second had more plastic. In both tests on the first package, the fire reached a peak heat release rate at approximately four minutes. However, they reached zero at different times (greater than 30 minutes versus approximately 20 minutes). In the two tests on the second package, the time of peak heat release was different (a high peak at four minutes versus a relatively low peak at 10 to 20 minutes), but they both reached zero at approximately the same time (50 minutes).

The third fuel package was designed to represent normal combustibles that might be in control or computer rooms, and consisted primarily of cardboard and stacked paper, with some crumpled paper. Total mass was about 7.9 kg. In both tests, the fire reached a peak heat release rate in approximately two minutes, but reached zero at different times (16 minutes versus 20 minutes).

The fourth fuel package was designed to represent mixed waste that might be found in a control room, computer room, security room, or similar location. It consisted primarily of a plastic trash can filled with paper and rags. Total mass was about 1.6 kg. In both tests, the fire reached a peak heat release rate in approximately three minutes and remained relatively steady for most of the duration of the fire, but reached zero at different times (54 minutes versus 70 minutes).

The fifth fuel package was designed to represent larger industrial waste containers that might be found in a variety of places in an industrial facility. It consisted primarily of a large plastic receptacle filled with wood, cardboard, paper, and oily rags. Total mass was about 6.5 kg. Only one test was conducted with this fuel package, and the fire reached two separate peak heat release rates (at 35 and 50 minutes) and decayed toward reaching zero at 80 minutes.

The preceding test data were reviewed and a probability distribution for the fire duration was developed based on engineering judgment. This distribution is characterized by 10% to 90 % hazard levels of 10 minutes and 60 minutes, respectively (i.e., it was concluded that 10% of the fires would result in a target exposure duration of less than 10 minutes and 90% of the fires would result in a target exposure duration of less than 60 minutes). These values were fitted to a lognormal distribution with a mean and standard deviation of 3.192 and 0.6943, respectively. The mean of this distribution is approximately 31 min, the median (50th percentile) is approximately 24 min, and the error factor (i.e., the ratio of the 95th percentile over the median) is about 3.1. The resultant probability distribution is presented in Table D2.1-1 as the probability of target exposure durations over a set of discrete intervals. The 30-minute design basis fire duration mandated in 10 CFR 71.73 (Ref. D4.2.2) corresponds to the 62nd percentile value of this distribution.

Table D2.1-1. Probability Distribution for Fire Duration - Without Automatic Fire Suppression

Fire Duration (min)	Cumulative Probability	Fire Duration Interval (minutes)	Interval Probability[a]
10	0.1	0 to 10	0.1
20	0.39	10 to 20	0.29
30	0.62	20 to 30	0.23
40	0.76	30 to 40	0.14
50	0.85	40 to 50	0.09
60	0.903	50 to 60	0.053
70	0.936	60 to 70	0.033
90	0.97	70 to 90	0.034
120	0.989	90 to 120	0.019
150	0.9956	120 to 150	0.0066
180	0.998	150 to 180	0.0024
210	0.999	180 to 210	0.001
270	0.99974	210 to 270	0.00074
360	0.99995	270 to 360	0.00021
∞	1	>360	5E-05

NOTE: [a] The interval probability is the difference between the cumulative probability at the top of the interval and the cumulative probability at the bottom of the interval.

Source: Original

D2.1.1.3 Fire Duration with Automatic Suppression

The second uncertainty distribution that was developed is for fires where automatic suppression is available. There were only a limited number of tests conducted for this case.

Factory Mutual Research Corporation conducted tests for large-scale configurations of cable trays, as discussed in the previous sections. In addition to the tests conducted without suppression, a number of tests were conducted with suppression. NUREG/CR-4679 (Ref. D4.1.53, pp. 26-31) provides detailed results for six of these “extinguishment tests.” All these tests involved a configuration of 12 fully loaded horizontal trays in two stacked tiers. Two of the six also involved the addition of two fully loaded vertical cable trays. The cables were polyvinyl chloride (PVC) - jacket with polyethylene insulation. The results of the first four tests were that the fires reached their peak heat release rates at 8, 9, 12, and 12 minutes. The associated times when the heat release rate dropped to zero were 10, 12, 16, and 29 minutes, respectively. The results of the final two tests were peak heat release rates at 9 and 16 minutes, with zero being reached at 24 and 36 minutes, respectively.

These were the only extinguishment tests reported in the references. Therefore, an analysis of a wooden box-type fire conducted by Parsons also was examined. This is not an actual test, but rather a calculation of a “typical” fire where credit was given for the actuation of fire suppression. The calculation gave a peak heat release rate occurring at seven minutes and extending to 15 minutes. The calculation showed the fire decaying towards zero at approximately 20 minutes.

These test data were reviewed and a probability distribution for the fire duration was developed based on engineering judgment. Although the data are somewhat sparse, they were taken in the overall context of how the actuation of suppression affected the tests conducted and how that compared to the free-burn tests. This was extrapolated to the other free-burn tests. It was judged likely that the operation of automatic suppression would have little effect on the lower end of the distribution, as such fires would likely burn out without actuating suppression. However, there would be a significant effect for the longer fires. It was concluded that a reasonable estimate of the 10 to 90 % hazard levels was 10 minutes and 30 minutes (i.e., it was concluded that it was a reasonable interpretation of the data to state that 10 % of the fires would result in target exposure duration of less than 10 minutes and 90 % of the fires would result in target exposure duration of less than 30 minutes). These values were fitted to a lognormal distribution with a mean and standard deviation of 2.849 and 0.4286, respectively. The resultant uncertainty distribution is presented in Table D2.1-2 as the probability of target exposure durations over a set of discrete intervals.

Table D2.1-2. Probability Distribution for Fire Duration - With Automatic Fire Suppression

Fire Duration (min)	Cumulative Probability	Fire Duration Interval (min)	Interval Probability[a]
10	0.1	0 to 10	0.1
15	0.37	10 to 15	0.27
20	0.63	15 to 20	0.26
25	0.81	20 to 25	0.18
30	0.901	25 to 30	0.091
40	0.975	30 to 40	0.074
50	0.993	40 to 50	0.018
60	0.9982	50 to 60	0.0052
80	0.9998	60 to 80	0.0016
100	0.99998	80 to 100	0.00018
∞	1	>100	2E-05

NOTE: [a] The interval probability is the difference between the cumulative probability at the top of the interval and the cumulative probability at the bottom of the interval.

Source: Original

D2.1.2 Uncertainty in Fire Temperature

As used in the fire fragility analysis, the fire temperature is the effective blackbody temperature of the fire. This temperature implicitly accounts for the effective emissivity of the fire, which for large fires approaches a value of 1.0 (Ref. D4.1.61, p. 2-56). A review of the available fire temperature data for liquid and solid fuels is discussed below.

Experimental measurements of liquid hydrocarbon pool fires with radii from 0.25 to 40.0 m indicate effective blackbody radiation temperatures between 1,200°K and 1,600°K (927°C and 1,327°C) (Ref. D4.1.61, p. 2-56). Testing of rail tank cars engulfed in a liquid hydrocarbon pool fire indicates an effective blackbody temperature of 816°C to 927°C (1,089°K to 1,200°K) (Ref. D4.1.2).

Heat release data for combustible solid materials such as wood, paper, or plastic are plentiful, but fire temperature data have generally not been presented. However, *The SFPE Handbook of Fire Protection Engineering* (Ref. D4.1.61, pp. 3-82 to 3-87) discusses the hot gas temperatures associated with fully-developed compartment fires that do include combustion of solid materials. Fully-developed fires involve essentially all combustible material in a compartment, so the peak hot gas temperature should be reasonably indicative of the *effective* fire temperature. The data indicate typical peak temperatures between 400°C and 1,200°C (750°F and 2,190°F). (The 400°C value applies to small, short duration fires and is too low to represent a true fire temperature.)

Fires within one of the YMP facilities are likely to involve both combustible solid and liquid materials. Judgment suggests that most postulated fires should generally resemble the compartment fires discussed in *The SFPE Handbook of Fire Protection Engineering* (Ref. D4.1.61, Section 2, Chapter 7). This implies that the assigned temperature distribution should be strongly influenced by the 400°C and 1,200°C range. However, combustible liquids (e.g., diesel fuel in a site transporter) may also contribute significantly to some fires, so the upper bound of the fire temperature distribution should include the higher temperatures indicated by the pool fire data. Based on this reasoning, the fire temperature distribution is normally distributed with a mean of 1,072°K (799°C) and a standard deviation of 172°K. The mean of this distribution is approximately equal to the transportation cask design basis fire temperature of 800°C mandated in 10 CFR 71.73 (Ref. D4.2.2).

This fire temperature probability distribution has a value of 400°C for the 5th percentile and 1,327°C for the 99.9th percentile. The first value represents the lower end of the compartment fire temperature range while the second corresponds to the upper end of the liquid pool fire effective blackbody temperature range. Therefore, the distribution applies to fires involving both liquid and solid fuels.

It should be noted that data from fire testing indicate that the fire temperature is not constant over the duration of the fire. The fire temperature generally increases to a peak value and then decreases considerably as the combustible material is consumed. In the fire fragility analysis, herein, the fire temperature is treated as constant, which tends to increase the maximum target temperature.

D2.1.3 Correlation of Fire Temperature and Duration

Testing has shown that fire temperature and duration are negatively correlated. Intense fires with high fire temperatures tend to be short-lived because the high temperature results from very rapid burning of the combustible material. In contrast, long duration fires generally result from slower burning of the combustible material. In the probabilistic fire fragility analysis discussed below, the fire temperature and duration were correlated with a conservative correlation coefficient of -0.5. It is conservative because this correlation allows some fires that have both a high temperature and long duration.

D2.1.4 Uncertainty in the Thermal Response of the Canister

The probability distributions discussed in Section D2.1.1 characterize the uncertainty in the fire severity. In order to determine the probability that a canister fails due to a fire, models are needed to calculate the uncertainty in the thermal response of the container to a fire and the uncertainty in the failure temperature of the container.

The following sections describe the two simplified heat transfer models used to determine the thermal response of the canister to the fire. The heat transfer models have been simplified in order to allow a probabilistic analysis using Monte Carlo sampling. The two models discussed below apply to bare canisters or canisters inside a waste package, transportation cask, or a canister transfer machine (CTM) shielded bell. The simplified model was validated by comparison with a more complete model as discussed in Section D2.1.4.3.

D2.1.4.1 Heat Transfer to Bare Canisters

Bare canisters near or engulfed in a fire can be heated primarily by two heat transfer mechanisms: convection and radiation. Convection heating occurs when hot gases from the fire circulate and come into contact with the canister surface. Due to gravitational effects, the hot gases from the fire are expected to rise and collect near the ceiling of the room. Thus, unless a canister is engulfed in the fire, the hot gases are unlikely to come into direct contact with the canister, and radiation should be the dominant mode of heating. Further, radiation from the flame (luminous portion of the fire gases) is expected to far exceed radiation from the hot gas layer near the ceiling. For that reason, radiative heating by the hot gas layer is not considered in the fragility analysis. The heat transfer model described in the following sections are believed to capture the important aspects of the heat transfer from the fire.

Due to substantial conduction within the metal wall of the canister, the canister wall is modeled as a single effective temperature (thin-wall approximation) during heatup. Using this approach, the canister temperature (T_c) was advanced in time using the following Euler finite-difference formulation (Equation D-5):

$$T_c = \frac{q_{c,net}\Delta t}{m_c c_{p,c}} + T_{c,i} \qquad \text{(Eq. D-5)}$$

where

m_c	=	mass of the canister wall
$c_{p,c}$	=	specific heat of the canister material
Δt	=	time step
$T_{c,i}$	=	canister temperature at the beginning of the time step, and
$q_{c,net}$	=	net rate of energy deposition into the canister.

The net rate of energy deposition into the canister during the fire is given by the following equation (Equation D-6):

$$q_{c,net} = q_{r,fire} + q_{c,fire} - q_{r,f} \tag{Eq. D-6}$$

where

$q_{r,fire}$ = radiative heat transfer to the canister from the fire

$q_{c,fire}$ = net convective heat transfer to the canister (positive if the canister is engulfed by the fire and negative if the canister is not engulfed by the fire)

$q_{r,f}$ = radiative heat transfer from the canister to material stored in the canister.

The terms on the right-hand-side of this equation are defined below.

An earlier formulation of Equation D-6 included convective heat transfer from the canister wall to the gas inside the canister and from this gas to the spent fuel inside the canister. The addition of this heat transfer term did not significantly affect the heating rate of either the canister or the fuel, but did significantly increase the calculation time for the analysis. For that reason, convective heat transfer to the gas inside the canister was not included in the subsequent probabilistic analysis.

In this analysis, the important parameters are: (1) the fire temperature, size, and location relative to the canister, (2) treatment of the fire surface as a blackbody, and (3) treatment of the canister surface as diffuse and gray. Thus, the net rate of radiative heat transfer to the canister surface, $q_{r,fire}$, is given by Equation D-7:

$$q_{r,fire} = \varepsilon_c A_c F_{c\text{-}fire} F_s \sigma \left(T_{fire}^4 - T_c^4\right) \tag{Eq. D-7}$$

where

ε_c = emissivity of the canister surface

A_c = surface area of the canister

$F_{c\text{-}fire}$ = view factor between the canister and the fire, which is the related to the fraction of radiation leaving the fire that strikes the canister surface

F_s = suppression scale factor (discussed below)

σ = Stefan-Boltzmann constant

T_{fire} = effective blackbody temperature of the fire

T_c = canister temperature.

In Equation D-6, $q_{c,fire}$ is the energy input due to convective heating from the fire, which is given by Equation D-8:

$$q_{c,fire} = A_c F_s h_{conv} \left(T_{fire} - T_c\right) \tag{Eq. D-8}$$

where h_{conv} is the convective heat transfer coefficient and all other terms are defined as above.

The final term in Equation D-6 is the rate of heat transfer from the canister to the spent fuel or high level waste. This term is given by the following equation (Equation D-9):

$$q_{r,f} = \frac{A_c F_{c\text{-}f} \sigma \left(T_c^4 - T_f^4\right)}{1/\varepsilon_c + 1/\varepsilon_f - 1} \qquad \text{(Eq. D-9)}$$

where $F_{c\text{-}f}$ is the view factor between the canister and the fuel, ε_f is the emissivity of the fuel, and T_f is the temperature of the fuel being heated by the canister (outer portion of the fuel).

As the canister becomes hotter and heat is transferred to the fuel, the fuel temperature will also increase according to the following equation (Equation D-10):

$$T_f = \frac{(q_{r,f} + q_{DH})\Delta t}{m_f c_{p,f}} + T_{f,i} \qquad \text{(Eq. D-10)}$$

where q_{DH} is the decay heat generated in the fuel, m_f is the mass of fuel heated by the canister (outer portion of the fuel), $c_{p,f}$ is the specific heat of the fuel, and $T_{f,i}$ is the fuel temperature at the beginning of the time step.

Equation D-10 uses the mass of fuel being heated by the canister and the corresponding decay heat in this portion of the fuel. This equation ignores heat transfer from the heated fuel to unheated fuel. That is, there is no energy exchange between the outer fuel and the inner fuel.

The fuel mass to use in Equation D-10 can be estimated by calculating the thermal penetration depth within the fuel during the fire. In a number of previous studies (for example, (Ref. D4.1.25)), the fuel region inside the canister has been treated as a homogeneous material with effective thermal properties. The effective thermal properties used in these studies were determined for many different fuel configurations based on the results from detailed thermal analyses. Table D2.1-3 presents the effective thermal properties for 21-PWR fuel in the TAD canister (Ref. D4.1.25).

Table D2.1-3. Effective Thermal Properties for 21-PWR Fuel in a TAD Canister

Property	Value
Density, ρ	3,655 kg/m^3
Specific Heat, c_p	438 J/kg K
Thermal Conductivity, k	4.29 W/m K
Thermal Diffusivity, α	2.6×10^{-6} m^2/sec

NOTE: PWR = pressurized water reactor; TAD = transportation, aging, and disposal (canister).

Source: Ref. D4.1.25, Table 17, and Equation 2 of Section 6.2.2

Based on the effective thermal properties listed in the table, estimation of the thermal penetration depth during a typical fire is given by the following equation (Equation D-11):

$$\delta = \sqrt{\alpha t} \qquad \text{(Eq. D-11)}$$

where α is the effective thermal diffusivity and t is the time (3,600 seconds). Based on the effective thermal diffusivity shown in the table, a thermal penetration depth of approximately 9.5 cm is calculated. The fuel volume corresponding to this penetration depth is calculated by multiplying the canister interior surface area by the penetration depth. The effective fuel mass is then calculated by multiplying this volume by the effective density of the fuel. The resulting fuel mass is approximately 9,700 kg.

D2.1.4.2 Heat Transfer to a Canister inside a Cask, Waste Package, or Shielded Bell

The calculation of the heating of a canister inside another container or structure is slightly more complex than that for a canister directly exposed to fire. When inside another container, the canister is not directly heated by the fire. Rather, the container is first heated by the fire and then the interior surface of the heated container radiates heat to the canister and also convects heat to any air or other gas in the annular region between the outer container and canister. When there are multiple heat transfer barriers (e.g., the waste package, which has an outer barrier and an inner barrier), heat transfer between the barriers must also be considered. The following discussion includes the presence of an inner and outer barrier, as is the case for a waste package.

The calculation of canister heating was accomplished by first calculating the temperature of the outer barrier when exposed to a fire. Then, the energy radiated from the outer barrier to the inner barriers was calculated. Next, the energy radiated from the inner barrier to the canister was calculated. Models that included convective heat transfer to and from the gas in the annular spaces between these regions demonstrated that convective heating and cooling had little effect on the heating of the canister, but caused calculation times to be significantly longer. As a result, the convective heat transfer was removed from the models and the temperature increase of the inner barrier and canister were calculated based on radiative heating only.

It should also be noted that many transportation casks have neutron or gamma shielding composed of a low melting point material such as borated polyethylene. This material is likely to melt very quickly so its effect on heat transfer was not considered in the model. In reality, this layer of material would have a substantial resistance to heat transfer, at least initially. Ignoring this thermal resistance is therefore conservative.

The heating of the outer barrier is calculated in the same general manner as that of a bare canister exposed directly to a fire. Due to the substantial conduction within the metal barrier, the thin-wall approximation was applied. Using this approach, the outer barrier temperature (T_{ob}) was advanced in time using the following Euler finite-difference formulation (Equation D-12):

$$T_{ob} = \frac{(q_{ob} - q_{ib})\Delta t}{m_{ob} c_{p,ob}} + T_{ob,i} \qquad \text{(Eq. D-12)}$$

where

q_{ob} = radiation and convection to the outer barrier from the fire

q_{ib} = radiation to the inner barrier from the outer barrier

m_{ob} = mass of the outer barrier

$c_{p,ob}$ = specific heat of the outer barrier

Δt = time step

$T_{ob,i}$ = outer barrier temperature at the beginning of the time step.

Equation D-12 does not consider convective heat transfer to the air inside the container. Initial calculations showed that convective heat transfer to the air in the container would be small compared to the radiation heat loss term, so convective heat transfer was neglected.

If (1) the fire temperature, size, and location relative to a container are known, (2) the fire surface can be treated as a blackbody, and (3) the outer barrier surface can be considered diffuse and gray, then the net rate of radiative heat transfer to the outer barrier surface (q_{ob}) can be approximated as Equation D-13:

$$q_{ob} = \varepsilon_{ob} A_{ob} F_{fc} F_s \sigma \left(T_f^4 - T_{ob}^4 \right) \qquad \text{(Eq. D-13)}$$

where

ε_{ob} = emissivity of the outer barrier surface

A_{ob} = surface area of the outer barrier

F_{fc} = view factor for radiative heat transfer, which is related to the fraction of radiation leaving the fire that strikes the outer barrier surface

F_s = suppression scale factor (discussed below)

σ = Stefan-Boltzmann constant

T_f = fire (flame) temperature

T_{ob} = temperature of the outer barrier.

Once the temperature of the outer barrier is known, the heating of the inner barrier can be found in the same manner. Instead of a fire temperature, the temperature of the heated outer barrier is used and the net rate of radiative heat transfer from the outer barrier interior surface to inner barrier (q_{ib}) can be approximated as Equation D-14:

$$q_{ib} = \frac{A_{ob} F_{oi} \sigma \left(T_{ob}^4 - T_{ib}^4 \right)}{1/\varepsilon_{ib} + 1/\varepsilon_{ib} - 1} \qquad \text{(Eq. D-14)}$$

where

ε_{ib} = emissivity for of the inner barrier

F_{oi} = view factor for radiation between the outer and inner barriers (discussed below)

T_{ib} = inner barrier surface temperature.

The temperature of the inner barrier is calculated using an equation similar to Equation D-12; however, in this equation, the thermal radiation incident on the inner barrier comes from the outer barrier rather than the fire and the heat loss from the inner barrier is to the spent fuel or high level waste canister.

Finally, the temperature of the canister is calculated using the following equation (Equation D-15), which has a form similar to Equation D-12:

$$T_c = \frac{(q_{ib} + q_{DH})\Delta t}{m_c c_{p,c}} + T_{c,i} \qquad \text{(Eq. D-15)}$$

where q_{DH} is the total decay heat generated by the contents of the canister and all other terms are defined as in preceding equations.

In Equation D-15, the heat capacity of the contents of the canister is conservatively neglected so that all decay heat is transmitted to the canister wall. In reality, some fraction of the decay heat would be transmitted to the contents of the canister (e.g., the spent fuel or high level waste), increasing the temperature of the contents. Neglecting this term is conservative since it increases the temperature increase of the canister itself.

Note also that, in order to simplify the model, heat transfer from the canister to its contents is ignored in Equation D-15. In reality, some heat would be transferred from the canister wall to the spent fuel or high level waste inside the canister. Neglecting this heat removal is conservative since it increases the temperature increase of the canister.

Unlike the bare canister case in which heating of the canister ends when the fire ends, heating of a canister that is inside other containers will increase after the fire ends as heat is transmitted from the heated outer and inner barrier. After the fire has been extinguished, heat will be lost by the outer barrier due to a combination of radiation to cooler surfaces and convection to the air in the room. A temperature of 400°K was used as the surface and air boundary condition. The surfaces were modeled as blackbodies in the radiation heat transfer calculation. Convective heat transfer was calculated based on a heat transfer coefficient of 2.0 W/m^2 K. The fragility analysis showed that the predicted canister failure probability was not sensitive to either the boundary condition temperature or the convective heat transfer coefficient.

D2.1.4.3 Validation of the Simplified Heat Transfer Models

In order to validate the simplified heat transfer models discussed above, results were compared to results calculated using more detailed models. In one such comparison, results calculated using the model for heating of a canister in a waste package were compared to the results from a similar ANSYS calculation (Ref. D4.1.25, Attachment V). ANSYS is a finite-element analysis software application use in nuclear facility and non-nuclear industrial applications to model temperature evolutions of complex systems. The simplified model was set up to match the inputs to the ANSYS calculation as closely as possible. The only differences between the two included:

- The ANSYS run was made with temperature-dependent specific heats whereas average specific heats were used in the simplified model.
- The ANSYS run treated the TAD canister and its contents as a homogeneous material with average properties, whereas the simplified model treated the TAD canister but ignored heat transfer to its contents.

Figure D2.1-1 shows a comparison of the calculated time-dependent temperatures from these two calculations. The figure shows that the simplified model accurately predicts the results from the more detailed analysis. Because heat transfer from the TAD canister to its contents is ignored in the simplified model, the canister reaches slightly higher temperatures with the simplified model compared to the more detailed model.

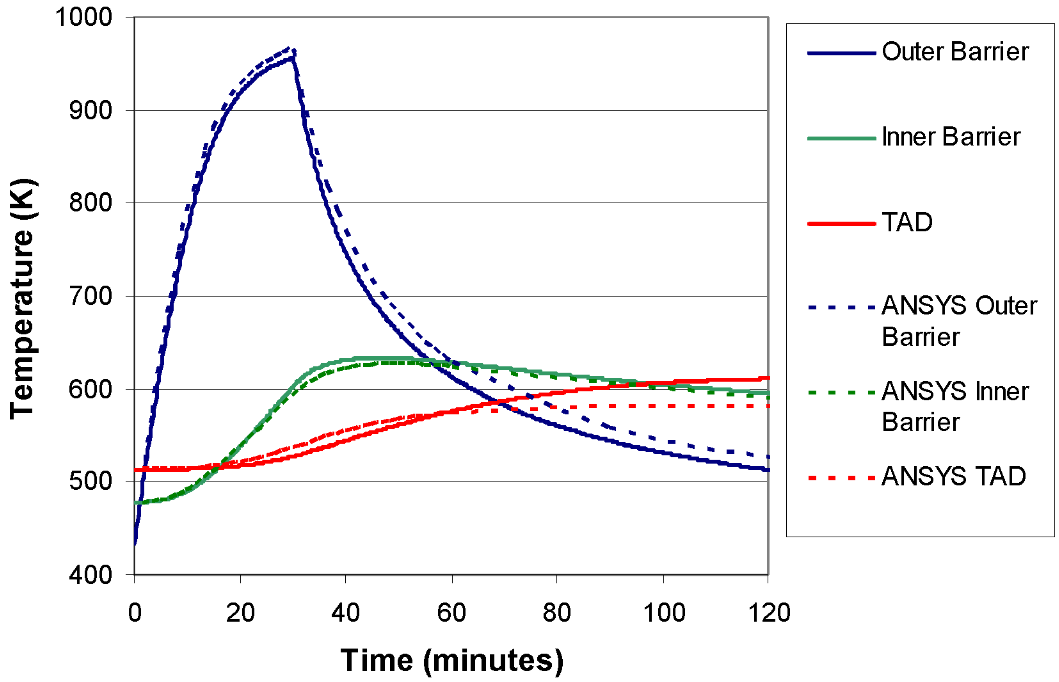

NOTE: TAD = transportation, aging, and disposal (canister).

Source: Original

Figure D2.1-1. Comparison Between Results Calculated Using the Simplified Heat Transfer Model and ANSYS – Fire Engulfing a TAD Canister in a Waste Package

A similar comparison was made between the results reported in the HI-STAR safety analysis report (SAR) (Ref. D4.1.38, Table 3.5.4) and results calculated using the simplified model. These calculations simulated a design basis 30-minute fire. The maximum canister temperature reported in the HI-STAR SAR was 419°F (215°C). This temperature was predicted to occur approximately 3 hours after the start of the fire. The simplified model predicted a peak canister temperature of 213.5°C at approximately 4 hours after the start of the fire. This comparison again demonstrates the accuracy of the simplified model in predicting the maximum canister temperature due to the fire.

Detailed ANSYS calculations were not performed for the bare canister configuration. However, it is possible to infer the accuracy of the simplified bare canister model based on the accuracy of the simplified model in predicting the thermal response of the outer barrier in the waste package configuration. As shown in Figure D2.1-1, the simplified heat transfer accurately predicted the thermal response of the outer barrier both during the 30-minute fire and after.

D2.1.4.4 Heat Transfer Model Inputs and Uncertainties

The heat transfer models discussed in Sections D2.1.4.1 and D2.1.4.2 include a large number of input parameters. Some of these parameters are known to a high degree of confidence whereas others are considered to be uncertain. This uncertainty was explicitly considered in the probabilistic analysis discussed in Section D2.1.1. The following sections discuss the major inputs to the models and the treatment of the uncertainty in these inputs.

D2.1.4.4.1 View Factor

The radiation view factor from the container (e.g., cask or waste package) to the fire can be calculated if the size of the fire and distance between the fire and the container can be determined. The size (height and width) of the fire can be approximated using published correlations in the Society of Fire Protection Engineering (SFPE) handbook (Ref. D4.1.61, Section 1, Chapter 6). The distance between the fire and the container depends on the location of combustible materials and ignition sources relative to the container.

Since the location of combustible materials and ignition sources relative to the container is difficult to predict and would vary from one room to another, a conservative approach in which the container was engulfed by the fire is followed. For a container completely engulfed by the fire the view factor is essentially 1.0. This is conservative for the long vertically-oriented containers because even an engulfing fire may engulf only the lower portion of the container.

A view factor of 1.0 was applied only to the cask, waste package, or a shielded bell that encase a canister. Bare canisters are treated differently. Since a canister is only bare as it is being withdrawn from a cask or inserted into a waste package, only a portion of the canister could be exposed to the fire at any given time. In this case, the view factor is given by fraction of the canister actually exposed to the fire. This fraction depends on the space between the top of the cask or waste package and the ceiling of the loading or unloading room. Generally, this fraction would be considerably less than 50 %.

The radiation view factor between concentric cylinders (e.g., the inner and outer barrier of a waste package) can be estimated very easily if the cylinders are very long compared to their diameters. Under this condition, which is true of most configurations of interest in the current study, the view factor can be approximated by D_i/D_o where D_i and D_o are the inner and outer diameters of the two cylinders (Ref. D4.1.63, Configuration C-63).

D2.1.4.4.2 Consideration of Fire Suppression on Canister Heating

The effect of fire suppression on canister heating is treated using a suppression scale factor. The suppression scale factor is included in the heat transfer equations as an adjustment to the rate of heat transfer to the canister from the fire. The value of the suppression scale factor used in the model is based on testing at the Building and Fire Research Laboratory, which is part of the National Institute of Standards and Technology (Ref. D4.1.31).

The Building and Fire Research Laboratory tests considered a range of fires and a range of sprinkler system spray densities. Results were presented for the net heat release rate from the fire both before and after actuation of the fire suppression system. The fire suppression scale factor implicitly includes consideration of the time delay before actuation of the fire suppression system and the effectiveness of the system. Rooms with early actuation and effective fire suppression would have a very small suppression scale factor, whereas rooms with delayed actuation and/or ineffective fire suppression would have a large suppression scale factor (upper bound of 1.0 when no suppression is present).

Because no credit is taken for fire suppression in this analysis, the fire suppression scale factor was set equal to 1.0 in all of the analyses discussed in this document.

D2.1.4.4.3 Convective Heat Transfer Coefficient during the Fire

In testing of containers engulfed in a fire, considerable variations in the convective heat transfer coefficient have been measured. Values as high as 30 W/m^2 K have been measured in vigorously burning pool fires (Ref. D4.1.51, pp. 19-21), although values on the order of 20 W/m^2K or less are considered more typical (Ref. D4.1.57, Table 3-2). For fire conditions in which the combustible material is burning more slowly, values on the order of 5 W/m^2 K or lower have been measured (Ref. D4.1.51, p. 19). To capture the potential variability in the convective heat transfer coefficient, a probability distribution for the convective heat transfer coefficient was included in the model. A normal distribution applies with a mean and standard deviation of 17.5 W/m^2 K and 4.2 W/m^2 K, respectively. This distribution yields practical upper and lower bound values (0.1 and 99.9th percentiles) of approximately 5 and 30 W/m^2K.

D2.1.4.4.4 Decay Heat

The canisters processed through the preclosure facilities will contain spent fuel with varying decay heat levels. Based on information provided in the safety analysis reports for transportation casks, a probability distribution was developed for the decay heat level in the canister. A normal distribution applies with a mean and standard deviation of 17 kW and 3 kW, respectively. This distribution yields practical upper and lower bound values (0.1 and 99.9th percentiles) of approximately 8 kW and 26 kW.

D2.1.4.4.5 Other Model Inputs

Other inputs required by the heat transfer model include (1) the thermal and physical properties of all materials, (2) the dimensions of the canister, cask, waste package, or shielded bell, (3) the initial temperatures of each layer, (4) decay heat generated within the canister, and (5) the post-fire convective heat transfer coefficient and temperature. The values for these input parameters are provided in Tables D2.1-4 through D2.1-7. The tables also provide a brief rationale or a reference for the values used in the analysis.

As shown in the tables, calculations were performed for two spent fuel canister wall thicknesses: 0.5 inches (0.0127 m) and 1.0 inch (0.0254 m). This was done for two reasons. First, initial calculations showed that the wall thickness greatly influences both the heating and failure of the canister. Second, a review of the available canister information indicated a range of canister thicknesses from 0.5 inches to 1 inch. A substantial fraction of the older transport cask designs have spent fuel canisters with wall thicknesses of 0.5 or 0.625 inches, whereas newer designs (e.g., the naval spent fuel canister or TAD canister) are expected to have a wall thickness of 1.0 inch.